

Diagrammatic Multiplet-Sum Method (MSM) Density-Functional Theory (DFT): Investigation of the Transferability of Integrals in “Simple” DFT-Based Approaches to Multi-Determinantal Problems

Abraham PONRA

Department of Physics, Faculty of Science, University of Maroua, P.O. Box 814, Maroua, CAMEROON

e-mail: abraPONRA@yahoo.com

Carolyne BAKASA

Technical University of Kenya, P.O. Box 52428-00200, Haile Selassie Avenue, Nairobi, KENYA

e-mail: carolyne.bakasa@gmail.com

Anne Justine ETINDELE

Higher Teachers Training College, University of Yaounde I, P.O. Box 47, Yaounde, CAMEROON

e-mail: anne.etindele@univ-yaounde1.cm

Mark E. CASIDA

Laboratoire de Spectrométrie, Interactions et Chimie théorique (SITh), Département de Chimie Moléculaire (DCM, UMR CNRS/UGA 5250), Institut de Chimie Moléculaire de Grenoble (ICMG, FR2607), Université Grenoble Alpes (UGA) 301 rue de la Chimie, BP 53, F-38041 Grenoble Cedex 9, FRANCE

e-mail: mark.casida@univ-grenoble-alpes.fr

Abstract

Static correlation is a difficult problem for density-functional theory (DFT) as it arises in cases of degenerate or quasi-degenerate states where a multideterminantal wave function provides the simplest reasonable first approximation to the true interacting wave function. This is also where Kohn-Sham DFT may also fail to be noninteracting v -representable (NVR). In contrast, Kohn-Sham DFT typically works well for describing the missing dynamic correlation when a single-determinantal reference wave function provides a good first approximation to the true interacting wave function. Multiplet sum method (MSM) DFT [*Theor. Chim. Acta* **4**, 877 (1977)] provides one of the earliest and simplest ways to include static correlation in DFT. MSM-DFT assumes that DFT provides a good description of single-determinant energies and uses symmetry and simple ansatzes to include the effects of static correlation. This is equivalent to determining the off-diagonal matrix elements in a small configuration interaction (CI) eigenvalue problem. We have developed a diagrammatic approach to MS-DFT facilitates comparison with wave function CI and so allows

educated guesses of off-diagonal CI matrix elements even in the absence of symmetry. In every case, an additional exchange-only ansatz (EXAN) allows the MSM-DFT formulae to be transformed into wave function formulae. This EXAN also works for transforming time-dependent DFT into time-dependent Hartree-Fock. Although not enough to uniquely guess DFT formulae from wave function formulae, the diagrammatic approach and the EXAN provide important constraints on any guesses that might be used. Some alternative guesses are tried out for problems concerning the ground and excited states of H_2 , LiH , and O_2 in order to assess how much difference might be involved for different DFT guesses for off-diagonal matrix elements.

1 Introduction

John P. Perdew is a giant figure in the field of density-functional theory (DFT). Speaking in the context of the present article, John Perdew embodies, for us, the need to comprehend the behavior of the *exact* exchange-correlation (xc) functional and the creation of *ab initio* xc functionals which satisfy as many of the conditions of the exact xc functional as possible. He, as we do, believes that this is the best way to ensure that the realm of applicability of a density-functional approximation extends all the way from atoms to solids, via molecules. The present, modest article, attempts in its own way imitate this admirable aspect of John's research in the sense of seeking structure and patterns which should be obeyed when building new theoretical models.

We wish now to talk about the unspeakable in Kohn-Sham DFT [1], or at least of an issue that is badly understood, and so rarely mentioned outside of specialized DFT circles. It is a problem of ground-state Kohn-Sham theory which resurfaces frequently in photochemical applications involving electronic excited states. This is the inability of even exact DFT to describe static correlation due to quasidegenerate states, made worse when using approximate xc functionals. Photochemical funnels (i.e., avoided crossings and conical intersections) are key for understanding many photophenomena and yet are exactly where static correlation is strongest. When these funnels are connected-<https://www.overleaf.com/project/64dfc992f85a039220b96748> to the ground state, then they also have a large impact on the ground-state potential energy surface (PES). The two most common DFT ways nowadays used to treat excited states are the time-dependent (TD) DFT and multiplet sum method (MSM) DFT. Each of these methods has its advantages and disadvantages. Here we will focus on MSM-DFT whose major disadvantage is its dependence on symmetry arguments. In fact, the principle motivation and *raison d'être* of the present article is to show how wave function theory (WFT) like diagrams may be developed for MSM-DFT, with the hope that this may then lead to the extension of MSM-DFT beyond high-symmetry problems. We show by example for H_2 , LiH , and O_2 that this provides a justification for substituting some double excitation terms with terms associated with single excitations (or, more properly, double replacement terms with single replacement terms).

The present reality is that most users of DFT are little educated in the fundamental theorems of DFT and may even be apathetic about this topic as long as their calculations allow them to solve their pet problem. *Yet formal theory matters!* The fundamental DFT theorems of Hohenberg-Sham [2] and the reformulation of DFT in terms of fictitious auxiliary orbitals by Kohn and Sham [1] present a well-defined exact theory for which xc-

DFT

xc

PES

WFT

functionals are to be developed. These functionals are to lead to a theory that behaves, not like WFT, but like formal DFT, obeying the exact conditions of exact DFT. The downside is that formal DFT can and does fail when trying to describe the ground states of certain types of systems. Hohenberg-Sham DFT assumed both N - and v -representability, which were later questioned. Put simply, given a positive reasonable-looking function which integrates to N , can we prove that it is the density of an N -electron wave function (the N -representability problem) and can we prove the existence of an external potential v whose ground state wave function leads to that positive reasonable-looking function which integrates to N (the v -representability problem)? The answer to the N -representability problem is “yes” [3] but the answer to the v -representability problem is “no” [4]. It is now relatively well-known that the need for v -representability may be circumvented by the Levy-Lieb constrained search reformulation of DFT [5, 6]. However Kohn-Sham DFT still requires noninteracting v -representability (NVR). As Levy had shown that there is always a noninteracting system with the same density as the interacting system, but it is not necessarily a ground state density [6]. Put more clearly, failure of NVR means that the lowest energy solution of the Kohn-Sham problem will have a lowest unoccupied molecular orbital (LUMO) which is lower in energy than the highest occupied molecular orbital (HOMO) or, in the jargon of the field, has “a hole below the fermi level.” Failure of NVR has been shown in some cases by taking the best possible from WFT and showing the impossibility of calculating the corresponding exact Kohn-Sham potential. It is also manifest, since it is easy to calculate, that the ground state of H_2 is in principle NVR. Nevertheless, a hole below the fermi level is often seen when using approximate xc-functionals and which we call effective failure of NVR [7]. This is exactly where Casida’s formulation of linear response TD-DFT can and does fail and which has an interesting connection with spin-wave instabilities. An ensemble formulation of DFT cannot fix this as it may lead to ensemble average geometries which are far from what we want if we are calculating realistic PESs. Alternatively, solving the NVR problem may seem to require an orbital dependence of the xc-functional which is also problematic and counter to the principles of Kohn-Sham DFT. These problems arise from quasidegenerate states and seem built into Kohn-Sham DFT, causing problems for ground-state DFT, but also particularly severe problems for DFT methods that treat excited states. (See Refs. [8, 7] for a more complete discussion of effective failure of NVR.) The need to introduce some sort of multideterminantal (MDET) nature into DFT seems manifest if we wish to overcome the effective violation of NVR problem. (See Ref. [9] for a lengthy recent discussion of current issues in DFT.)

NVR

HOMO
LUMO

MDET

A common way to try to incorporate some MDET character into DFT is to use symmetry breaking of the Kohn-Sham orbitals, with emphasis on different orbitals for different spin even in closed-shell systems. This is one way to obtain reasonable MDET-like PESs at the expense of other properties such as having the correct spin-densities. It is also difficult when using grid-based methods, where the underlying grid does not necessarily reflect the symmetry of the molecule, to prevent symmetry breaking. However symmetry breaking suffers from at least two obvious problems: (i) there may be (often are?) more than one way to break the symmetry of the wave function and different types of symmetry breaking might give the lowest energy for different atomic configurations and (ii) our experience with excited states indicates that not only are states more difficult to assign once symmetry is broken but calculated excitation spectra often simply become unreliable. Hence the need for a MDET extension without symmetry breaking.

SI

[A brief review of some other MDET extensions of DFT has been included in the Supplementary Information (SI) associated with this article.]

Our principle interest is in DFT tools that will help us treat the electronic excited states of molecules. Excited states, even more than ground states, are often fundamentally multideterminantal. The two most popular DFT methods for treating excited states are TD-DFT (see, e.g., [7]) and the older Ziegler-Rauk-Baerends-Daul MSM-DFT [10, 11]. Each of these methods has its pros and cons and, although the fundamental equations look very different, tend to give very similar answers in cases where both methods are applicable. TD-DFT obtains information about excited states by looking at the response of the charge density to an external applied electric field. In its usual formulation, it requires a single-determinantal reference state, so that it is only a MDET method for excited states. However spin-flip TD-DFT using a triplet reference state allows some incorporation of MDET character in the ground state. Much of the popularity of TD-DFT resides in the fact that it is easily automated. However it has difficulty teaing charge transfer and double excitations. MSM-DFT is the older method. It assumes that DFT provides a good description of dynamical correlation in states well described by a single-determinantal wave function and then uses symmetry arguments to obtain information about static correlation that gives rise to multiplet states. [The terms “dynamic” and “static” are imprecise “fuzzy” but still very useful terms. In DFT, dynamic correlation is often associated with atoms and static correlationn is associated with quasidegeneracies. In WFT, dynamic correlation is accounted for by many-body perturbation theory (MBPT) supposing that the unperturbed wave function is a good starting point. If this unperturbed wave function needs to be of MDET form, then we speak of static correlation.] MSM-DFT is more difficult to automate, being more strongly based upon physical and chemical intuition. In contrast to TD-DFT, MSM-DFT sometimes provides an easy way to handle double excitations and handles charge transfer excitations better than does TD-DFT. The present paper focuses on MSM-DFT. (Attempts to unite TD-DFT and MSM-DFT are briefly reviewed in the SI.)

MBPT

This article presents Feynman diagrams for analyzing terms in MSM-DFT. It is important to realize that our approach is different from other combinations of Feynman diagrams and DFT. It is now common in theoretical solid-state physics to do MBPT using DFT orbitals (e.g., Ref. [12] for a review). Feynman diagrams have also been used to analyze TD-DFT [13] and to add MBPT corrections to in dressed TD-DFT [14]. In contrast to these approaches, the present approach is very simple and (hopefully) transparent. We use the simplest type of Feynman diagrams—ones intended as an elementary baby step for pedagogical purposes in in Shavitt and Bartlett’s book (Chapter 4 of Ref. [15], pp. 90-129). Our goal is to seek analogies and patterns which will In particular, we will show that some double excitation terms may be calculated using only single excitations.

This article is organized in the following manner: The next section covers the basic theory used in the rest of the paper. Subsection 2.1 is review, but needed to establish notation and make sense of the otther subsections. A description of the WFT diagrams that we are using in this paper has been included in the SI. The reader who is not familiar with this type of Feynman diagrams is strongly urged to see the appropriate part of the SI. Subsections 2.2 and 2.3 are new and hence are included in the main text. The exchange-only anzatz (EXAN) in Subsec. 2.4 is not particulary new but has a special importance in the context of the present paper. Section 3 presents computational details. We then go on to present the results of some example calculations Sec. 4, notably for H₂ (Subsec. 4.1)

and for O₂ (Subsec. 4.3). An example calculation for LiH is presented in the SI. We will see that, while MSM-DFT terms cannot be replaced by their corresponding MSM-WFT terms, MSM-DFT terms are roughly equal when they correspond to MSM-WFT terms that are equal. This is a symmetry-independent result. Section 5 concludes.

2 Diagrammatic MSM-DFT

The objective of this section is to present a diagrammatic representation for MSM-DFT which closely parallels diagrammatic wave function theory. We will proceed by steps. We will first review the MSM with emphasis on the usual triplet/open-shell singlet application. A brief but essential review of a particular type of WFT diagrams introduced in Shavitt and Bartlett’s book primarily for pedagogical purposes (chapter 4 of Ref. [15], pp. 90-129), but which suits our present needs very well, is given in the SI and should be studied by reader’s not already familiar with this type of diagram. In a second step, we will modify these diagrams to include self-interaction terms (SITs). This is a crucial step because, although these SITs cancel out in WFT, they do not cancel out in DFT. Finally we will show how expansion of MSM-DFT expressions around a reference state lead to diagrams in close parallel with the WFT diagrams already presented.

SIT

2.1 Multiplet Sum Method

Ziegler, Rauk, and Baerends introduced the MSM-DFT to handle the problem of how to calculate multiplet splittings in excitation spectra using DFT [10]. Their particular emphasis was on the calculation of the energies of open-shell singlet excited states in closed shell molecules. They assumed that DFT gave a good description of states well described by a single determinantal wave function but is not able to describe states requiring a linear combination of quasidegenerate wave functions. That is, DFT is able to describe dynamic correlation well but fails at describing static correlation. On the other hand, WFT is able to describe static correlation with a wave function consisting of a few determinants but often requires millions of terms to obtain quantitative results for dynamic correlation. It makes sense to seek the best of both worlds by combining DFT and WFT in such a way that DFT captures most of the dynamic correlation while WFT catches the key static correlation. We will illustrate the basic arguments here for the two-orbital two-electron model (TOTEM). The TOTEM is adequate for treating both the problem of the ground and lower states of H₂, the lower diabatic states of LiH, and the ground and lower states of O₂. We will review these three applications in particular here. Note that Claude Daul extended MSM-DFT to the more complicated problem of spatial multiplet splittings in transition metal complexes [11].

We will mostly use orthonormal spin-orbitals when describing the formalism in this paper. These spin-orbitals are divided into occupied, unoccupied (virtual), and orbitals that are free to be either. We will make heavy use of the index convention,

$$\underbrace{a, b, c, \dots, g}_{\text{unoccupied}}, \underbrace{h, i, j, k, l, m, n, o}_{\text{occupied}}, \underbrace{p, q, \dots, x, yz}_{\text{free}} . \tag{1}$$

When necessary, spin will be indicated by an overbar for spin up and the absence of an

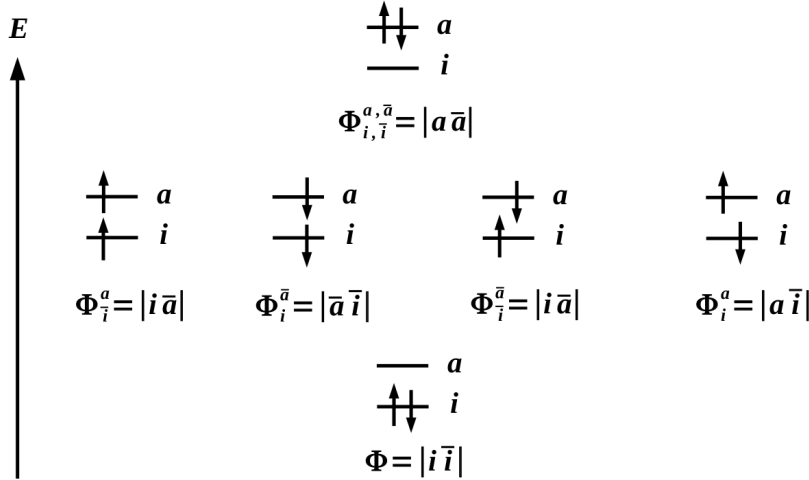


Figure 1: TOTEM state diagram when neglecting electron repulsions.

overbar for spin down. We also use the common convention,

$$|i_1, i_2, \dots, i_N\rangle = \frac{1}{\sqrt{N!}} \begin{vmatrix} \psi_{i_1}(1) & \psi_{i_2}(1) & \cdots & \psi_{i_N}(1) \\ \psi_{i_1}(2) & \psi_{i_2}(2) & \cdots & \psi_{i_N}(2) \\ \vdots & \vdots & \ddots & \vdots \\ \psi_{i_1}(N) & \psi_{i_2}(N) & \cdots & \psi_{i_N}(N) \end{vmatrix}, \quad (2)$$

for a single determinant, where (i) stands for the space and spin coordinates of electron i . In our TOTEM, we have just one occupied spatial orbital i and one unoccupied orbital a in the ground state. If we assume that the orbital energy of a is greater than that of i and neglect electron repulsions, then we get the state diagram of **Fig. 1**, consisting of six single-determinantal states.

In the presence, or absence, of the electron repulsion, the spin operators \hat{S}^2 and \hat{S}_z commute with the hamiltonian \hat{H} . Group theory then tells us that the eigenfunctions of the hamiltonian may be chosen as simultaneous eigenfunctions of these three operators, meaning that the eigenfunctions may be labeled using the spin quantum numbers (S, M) and that there will be $2S + 1$ degenerate functions for each value of S . However the single-determinantal solutions in Fig. 1 are not all spin eigenfunctions. In fact, non-spin eigenfunctions are still a possible valid choice of eigenfunctions of the hamiltonian when electron repulsion is neglected, but only because we are allowed to take linear combinations of degenerate states. Introducing electron repulsions will lift the degeneracy of the four states in the middle of Fig. 1 and these states will be labeled by S and M .

There are many different ways to deduce the spin eigenfunctions $\Psi_{S,M}$, but we wish to keep our presentation as simple as possible. So we will just note that the two-electron case is a special case where the spatial and spin parts of the spin eigenfunctions factor.

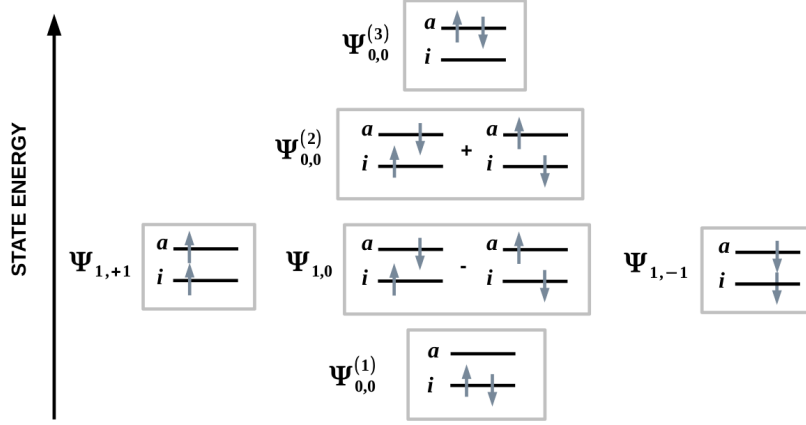


Figure 2: Generic TOTEM state diagram when electron repulsions are included. The wave functions $\Psi_{S,M}$ are labeled using the usual quantum numbers for the total spin (S) and for its projection on the z -axis (M).

This leads to the following spin eigenfunctions:

$$\begin{aligned}
\Psi_{1,+1} &= |i, a\rangle \\
&= \left[\frac{1}{\sqrt{2}} (i(1)a(2) - a(1)i(2)) \right] (\alpha(1)\alpha(2)) \\
\Psi_{1,0} &= \frac{1}{\sqrt{2}} (|i, \bar{a}\rangle - |a, \bar{i}\rangle) \\
&= \left[\frac{1}{\sqrt{2}} (i(1)a(2) - a(1)i(2)) \right] \left[\frac{1}{\sqrt{2}} (\alpha(1)\beta(2) + \beta(1)\alpha(2)) \right] \\
\Psi_{1,-1} &= |\bar{a}, \bar{i}\rangle \\
&= \left[\frac{1}{\sqrt{2}} (i(1)a(2) - a(1)i(2)) \right] (\beta(1)\beta(2)) \\
\Psi_{0,0} &= \frac{1}{\sqrt{2}} (|i, \bar{a}\rangle + |a, \bar{i}\rangle) \\
&= \left[\frac{1}{\sqrt{2}} (i(1)a(2) + a(1)i(2)) \right] \left[\frac{1}{\sqrt{2}} (\alpha(1)\beta(2) - \beta(1)\alpha(2)) \right]. \quad (3)
\end{aligned}$$

As the Pauli principle tells us that the total wave function must be antisymmetric, there are only two possibilities. In the first possibility, the spatial part of the wave function is antisymmetric and the spin part is symmetric. These are the triplet ($S = 1$) wave functions. They are energetically degenerate for a spin-free hamiltonian. The second possibility is that the spatial part of the wave function is symmetric and the spin part is antisymmetric. As there is only one way to do this, there is only one singlet ($S = 0$) wave function. Furthermore antisymmetry also means that electrons with the same spin avoid each other in space (Fermi hole) and so have a smaller electron repulsion energy than do electrons with the opposite spins because same spin electrons are, on average, farther apart. This is a common explanation of why triplet energies are usually lower than the corresponding singlet energies. This gives us the new generic state diagram given in **Fig. 2**. In principle, configuration mixing can occur between the three singlet

wave functions, $\Psi_{0,0}^{(1)}$, $\Psi_{0,0}^{(2)}$, and $\Psi_{0,0}^{(3)}$. The MSM assumes that we can neglect mixing of $\Psi_{0,0}^{(2)}$ with the other two singlet wave functions, either because of other symmetries (the case of H_2) or because of Brillouin's theorem (see the section on WFT diagram in the SI). Hence we need only be concerned with the open-shell singlet $\Psi_{0,0}^{(2)}$ and the three triplet states $\Psi_{1,+1}$, $\Psi_{1,0}$, and $\Psi_{1,-1}$. In fact, as only mixing between states with the same M quantum number is allowed, we have only to solve the small configuration interaction (CI) problem,

$$\begin{bmatrix} E[|a, \bar{i}|] & A \\ A & E[|i, \bar{a}|] \end{bmatrix} \begin{pmatrix} C_i^a \\ C_{\bar{i}}^{\bar{a}} \end{pmatrix} = E \begin{pmatrix} C_i^a \\ C_{\bar{i}}^{\bar{a}} \end{pmatrix}. \quad (4)$$

As $E_M = E[|a, \bar{i}|] = E[|i, \bar{a}|]$, this has two simple solutions, namely

$$\begin{aligned} E_S &= E_M + A \\ E_T &= E_M - A. \end{aligned} \quad (5)$$

Here E_M stands for the energy of a single-determinantal mixed symmetry state (i.e., one which is not a spin eigenfunction), E_S stands for the open-shell singlet energy, E_T stands for the open-shell triplet energy, and A is assumed to be real and positive. We will examine the nature of A in greater detail in the subsections below.

For now, let us focus on trying to get the best of two worlds, namely taking dynamical correlation from DFT and static correlation from WFT. A naïve way to do this is to simply replace E_M with the single-determinantal energy calculated in DFT. As will be illustrated in Sec. 4, this does not work because the three triplet states no longer have the same energy: $E[|i, a|] = E[|\bar{i}, \bar{a}|] \neq E[|i, \bar{a}|] - A$. The MSM solution to this problem is to rechoose the matrix element A so as to enforce degeneracy of the three triplet states. Hence,

$$A = E[|i, \bar{a}|] - E[|i, a|], \quad (6)$$

in the MSM. More generally, the MSM consists of finding as many symmetry conditions as possible linking off-diagonal energies with diagonal single-determinantal energies and then deduce formulae for the off-diagonal matrix elements. For example, both spin and spatial symmetry was taken into account in applying the MSM to the low-lying excited states of O_2 [16] as will be discussed in more detail in Sec. 4.

In some cases, there may not be enough symmetry to do this, so a few matrix elements are calculated explicitly *as they would be in WFT*. We will see in Sec. 4 that this latter approach is dangerous and should be avoided. In fact, the objective of the diagrammatic approach introduced in this article is to provide a tool for making better guesses as to how to calculate off-diagonal matrix elements in the absence of sufficient symmetry conditions. Another point is that the MSM implicitly assumes using the *same* MOs in constructing all of the states. This means first deciding on a reference configuration (preferably some type of state average without symmetry breaking) which provides a unique set of MOs to be used for calculating all of the MOs. These MOs are then used throughout the rest of the calculations at the price of possibly missing important relaxation effects.

2.2 SIT Diagrams

We use a simple type of WFT Feynman diagrams in this article. The reader not already familiar with this type of diagram is strongly urged to take a moment to review the explanation given in the SI before continuing to read the rest of this article.

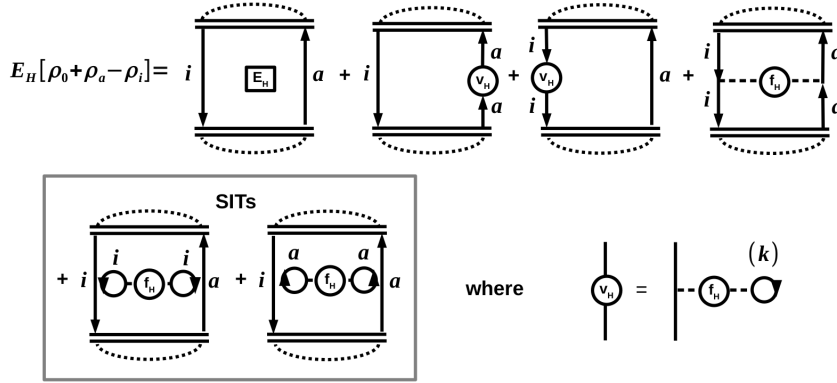


Figure 3: Diagrammatic expansion the Hartree part of $E[|i, a|]$. Here ρ_0 is the total charge density, $\rho_a = |\psi_a|^2$, and $\rho_i = |\psi_i|^2$. The SITs are a new type of diagram. Another point worth emphasizing is that the matrix element parts $E_H = E_H[\rho_0]$ and $v_H = v_H[\rho_0]$ depend upon the reference density, although other choices are possible. The kernel $f_H(1, 2) = 1/r_{1,2}$ is independent of the charge density.

Our interest is not WFT, but DFT. In particular, for simplicity, we are interested in Kohn-Sham DFT where the xc functional depends only upon the charge density and we will not talk about hybrid functionals (i.e., generalized Kohn-Sham DFT) although it seems trivial to modify our diagrammatic formalism to take hybrid functionals into account. Kohn-Sham DFT resembles Hartree theory more than Hartree-Fock because of the use of the classical Hartree energy,

$$E_H[\rho] = \frac{1}{2} \int \int \frac{\rho(1)\rho(2)}{r_{1,2}} d1d2. \quad (7)$$

This necessarily implies the presence of SITs, both self-interaction errors but also self-interaction corrections. In fact, SITs of various sorts are common in diagrammatic WFT where they go by the name of exclusion principle violating (EPV) terms and are recognizable by the presence of the same hole indices or the same particle indices at the same time (horizontal level in our diagrams). EPV terms are tolerated because they cancel each other, but this will no longer be the case in diagrammatic DFT. Making such terms explicit is also helpful because it forces us to deduce diagrams algebraically without second quantization and Wick's theorem. The result will be new types of diagrams not usually seen in diagrammatic WFT.

EPV

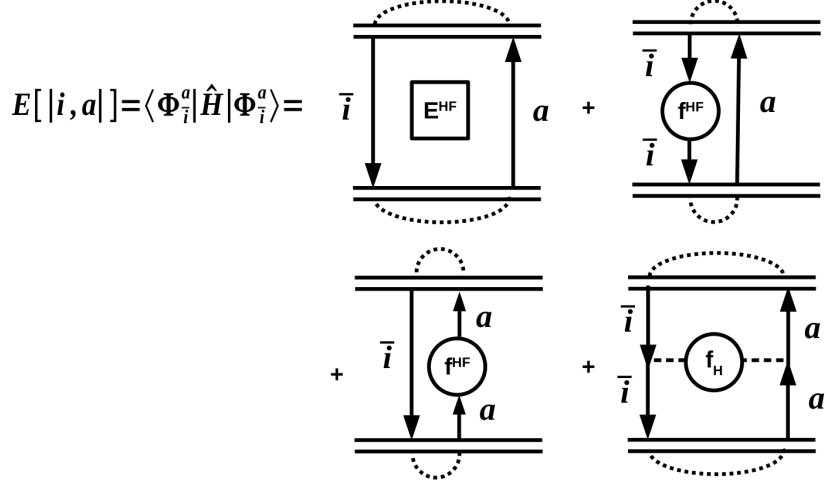


Figure 4: Diagrammatic evaluation of $E[|i, a\rangle]$.

Consider the specific case of evaluating $E[|i, a\rangle]$. This will include the Hartree term,

$$\begin{aligned}
E_H[\rho_0 + \rho_a - \rho_i] &= \frac{1}{2} \int \int (\rho_0(1) + \rho_a(1) - \rho_i(1)) \frac{1}{r_{1,2}} (\rho_0(2) + \rho_a(2) - \rho_i(2)) \\
&= \frac{1}{2} \int \int \rho_0(1) \frac{1}{r_{1,2}} \rho_0(2) d1d2 \\
&+ \int \int \rho_0(1) \frac{1}{r_{1,2}} \rho_a(2) d1d2 - \int \int \rho_0(1) \frac{1}{r_{1,2}} \rho_i(2) d1d2 \\
&- \int \int \rho_i(1) \frac{1}{r_{1,2}} \rho_a(2) d1d2 \\
&+ \frac{1}{2} \int \int \rho_i(1) \frac{1}{r_{1,2}} \rho_i(2) d1d2 + \frac{1}{2} \int \int \rho_a(1) \frac{1}{r_{1,2}} \rho_a(2) d1d2 \\
&= E_H[\rho_0] + \int v_H[\rho_0](1) \rho_a(1) d1 - \int v_H[\rho_0] \rho_i(1) d1 \\
&- (ii|f_H|aa) + \frac{1}{2}(ii|f_H|ii) + \frac{1}{2}(aa|f_H|aa). \tag{8}
\end{aligned}$$

The corresponding diagrams are shown in **Fig. 3**. As none of these diagrams arise from Wick's theorem, it might be assumed that some “guessing” occurs at this stage in writing down the diagrams. However there is actually little or no leeway in determining how to draw them. The only real questions might arise in the context of a *new type of diagram*, namely the SIT diagrams. We have not found any other way to draw them except as the Hartree interactions that they represent. There is a price to pay for this, namely that we need to add labels to indicate the specific orbitals involved and we violate *Rule 3* of the WF diagrams (see the SI) by using an unoccupied orbital index in loops that begin and end at the same time.

We can also follow the same procedure for the HF exchange energies, but using the one-electron reduced density matrix instead of the charge density. This gives the SITs shown in **Fig. 5** and **Fig. 7**. Note how these cancel out when the diagrams are evaluated

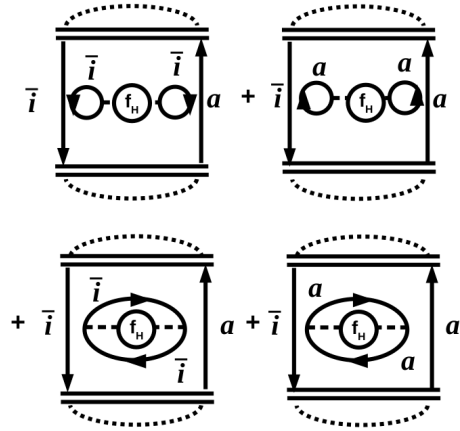


Figure 5: Explicit Hartree (direct) and exchange SIT diagrams implicit in **Fig. 4** for $E[|i, a|]$.

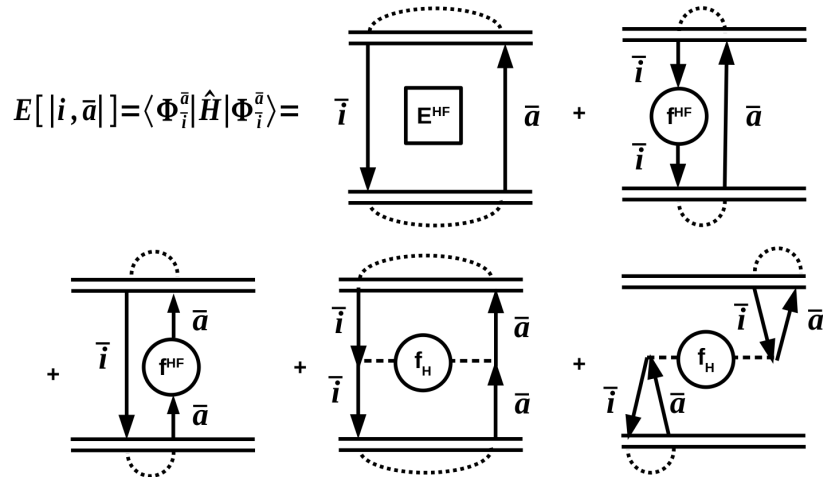


Figure 6: Diagrammatic evaluation of $E[|i, \bar{a}|]$.

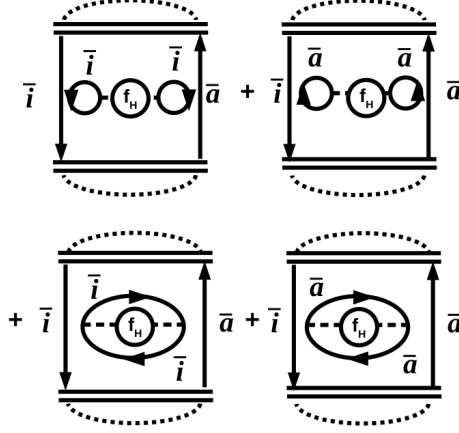


Figure 7: Explicit Hartree (direct) and exchange SIT diagrams implicit in **Fig. 6** for $E[|i, \bar{a}|]$.

according to the five rules given above. This will no longer be the case in the MSM-DFT diagrams.

2.3 MSM-DFT Diagrams

MSM-DFT diagrams are just like MSM-HF except that we have to keep the Hartree SITs and the HF exchange terms are replaced with DFT xc terms. The xc terms include the xc energy $E_{xc}[\rho^\uparrow, \rho^\downarrow]$, the xc potential $v_{xc}^\tau[\rho^\uparrow, \rho^\downarrow](1) = \delta E_{xc}[\rho^\uparrow, \rho^\downarrow] / \delta \rho^\tau(1)$, the xc kernel $f_{xc}^{\sigma, \tau}[\rho^\uparrow, \rho^\downarrow] = \delta^2 E_{xc}[\rho^\uparrow, \rho^\downarrow] / \delta \rho^\sigma(1) \delta \rho^\tau(2)$, and higher-order terms (HOT) such as $g_{xc}^{\xi, \sigma, \tau}[\rho^\uparrow, \rho^\downarrow] = \delta^3 E_{xc}[\rho^\uparrow, \rho^\downarrow] / \delta \rho^\xi(1) \delta \rho^\sigma(2) \delta \rho^\tau(3)$. We need to do an expansion around the zero-order densities ρ_0^\uparrow and ρ_0^\downarrow . This is possible once it is understood that a functional is just like a function of a vector except that instead of the vector having discrete indices for its components, the vector becomes a function (such as $\rho(x)$) with a continuous index (x) . This allows us to develop a calculus of variations [17] in close parallel with the multivariable calculus. In particular, we can carry out the calculus of variations analogue of a Taylor's expansion.

HOT

We will just give one example here and explain the relation with diagrams. Thus we consider the excitation of an electron from an occupied spin-down orbital i to an unoccupied spin-up orbital a . The spin-down density is reduced by an amount $-\rho_i = |\psi_i|^2$

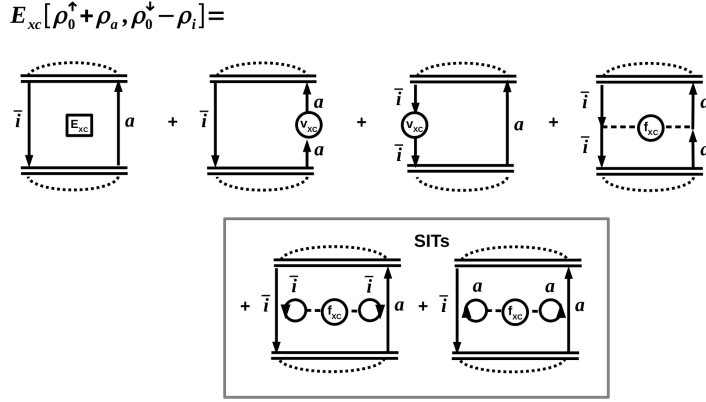


Figure 8: Explicit xc diagrams associated with $E[[i, a]]$. The matrix element symbols in the diagram have the same arguments, namely $[\rho_0^\uparrow, \rho_0^\downarrow]$. Notice that the spin indices on the xc potentials and kernels need not be specified as they are determined by the spins of incoming and outgoing lines.

while the spin-up density is increased by an amount $\rho_a = |\psi_a|^2$. We may then expand,

$$\begin{aligned}
E_{xc}[\rho_0^\uparrow + \rho_a, \rho_0^\downarrow - \rho_i] &= E_{xc}[[\rho_0^\uparrow, \rho_0^\downarrow]] \\
&+ \int \frac{\delta E_{xc}[\rho_0^\uparrow, \rho_0^\downarrow]}{\delta \rho_0^\uparrow(1)} \rho_a(1) d1 - \int \frac{\delta E_{xc}[\rho_0^\uparrow, \rho_0^\downarrow]}{\delta \rho_0^\downarrow(1)} \rho_i(1) d1 \\
&- \int \int \rho_i(1) \frac{\delta^2 E_{xc}[\rho_0^\uparrow, \rho_0^\downarrow]}{\delta \rho^\downarrow(1) \delta \rho^\uparrow(2)} \rho_a(2) d1 d2 \\
&+ \frac{1}{2} \int \int \rho_i(1) \frac{\delta^2 E_{xc}[\rho_0^\uparrow, \rho_0^\downarrow]}{\delta \rho^\downarrow(1) \rho^\downarrow(2)} \rho_i(2) d1 d2 + \frac{1}{2} \int \int \rho_a(1) \frac{\delta^2 E_{xc}[\rho_0^\uparrow, \rho_0^\downarrow]}{\delta \rho^\uparrow(1) \rho^\uparrow(2)} \rho_a(2) d1 d2 \\
&+ \text{HOT} \\
&= E_{xc}[\rho_0^\uparrow, \rho_0^\downarrow] \\
&+ \int v_{xc}^\uparrow(1)[\rho_0^\uparrow, \rho_0^\downarrow] \rho_a(1) d1 - \int v_{xc}^\downarrow(2)[\rho_0^\uparrow, \rho_0^\downarrow] \rho_i(1) d2 \\
&- (ii|f_{xc}^{\uparrow,\downarrow}[\rho_0^\uparrow, \rho_0^\downarrow]|aa) \\
&+ \frac{1}{2}(ii|f_{xc}^{\downarrow,\downarrow}[\rho_0^\uparrow, \rho_0^\downarrow]|ii) + \frac{1}{2}(aa|f_{xc}^{\uparrow,\uparrow}[\rho_0^\uparrow, \rho_0^\downarrow]|aa) \\
&+ \text{HOT}.
\end{aligned} \tag{9}$$

For the Hartree terms, the series truncates naturally after the second-order term as all HOT are zero. This is not true for xc terms, but nevertheless we will confine our development to no higher than the xc kernel. Equation [9] are shown in **Fig. 8**. Notice that only direct diagrams can appear in MSM-DFT as DFT is more Hartree-like than HF-like. Also $v_{xc}^\uparrow[\rho_0^\uparrow, \rho_0^\downarrow] = v_{xc}^\downarrow[\rho_0^\uparrow, \rho_0^\downarrow]$, $f_{xc}^{\uparrow,\uparrow}[\rho_0^\uparrow, \rho_0^\downarrow] = f_{xc}^{\downarrow,\downarrow}[\rho_0^\uparrow, \rho_0^\downarrow]$, and $f_{xc}^{\uparrow,\downarrow}[\rho_0^\uparrow, \rho_0^\downarrow] = f_{xc}^{\downarrow,\uparrow}[\rho_0^\uparrow, \rho_0^\downarrow]$, when $\rho_0^\uparrow = \rho_0^\downarrow$ as is normal for closed-shell molecules without any symmetry breaking.

We now wish to derive the diagrams for the A matrix element in MSM-DFT. To do this, we need the diagrammatic expansions for $E[[i, a]]$ and $E[[i, \bar{a}]]$ which are shown respectively in **Figs. 9** and **10**. Then, from Eq. 6 (represented diagrammatically in

$$A^{\text{DFT}} = E_{\text{KS}}[|i, a\rangle] = E_{\text{KS}}[|i, \bar{a}\rangle] =$$

Figure 11: Diagrammatic representation of the A matrix element in MSM-DFT. The xc matrix element symbols in the diagram have the same arguments, namely $[\rho_0^\uparrow, \rho_0^\downarrow]$.

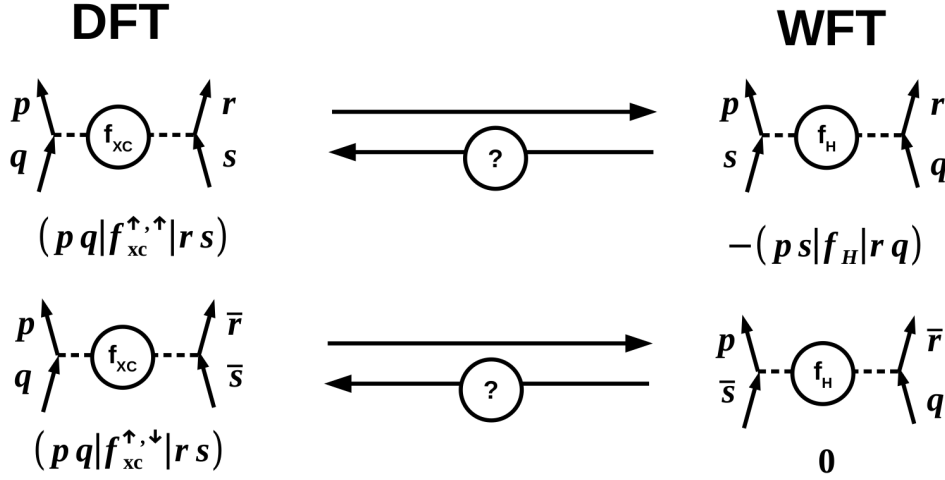


Figure 12: The exchange-only ansatz (EXAN).

Fig. 11),

$$A^{\text{DFT}} = (ii|f_{xc}^{\downarrow,\downarrow}[\rho_0^\downarrow, \rho_0^\uparrow]|aa) - (ii|f_{xc}^{\downarrow,\uparrow}[\rho_0^\downarrow, \rho_0^\uparrow]|aa). \quad (10)$$

2.4 Exchange-Only Ansatz

Up to this point, the only thing that is really new is the introduction of diagrams as a tool. It is also possible to check the MSM-DFT diagrams using the EXAN. This neglects antiparallel spin correlation and assumes that parallel spin correlation may be replaced by an exchange-type integral. The exact rules are given in **Fig. 12**. It allows us to take both the MSM-DFT and TD-DFT in the TDA and transform them into the corresponding HF-DFT or TD-HF equations. Note that this is not done by replacing DFT terms with terms of the same magnitude, but rather just shows parallels between the structure of the two theories. *If* we could go backwards and use the EXAN to make educated guesses for terms in MSM-DFT (or TD-DFT) from WFT, notably in the absence of symmetry arguments, then we would be able to show the usefulness of the diagrammatic analysis. The general formula for the WFT \rightarrow DFT mapping might be,

$$m(pr|f_H|qs) \rightarrow -m(pq|f_{xc}^{\uparrow,\uparrow}|rs) + n [(pr|f_H|qs) + (pq|f_{xc}^{\uparrow,\uparrow}|rs)] + \text{SITs} + \text{terms involving } f_{xc}^{\uparrow,\downarrow}, \quad (11)$$

assuming that $\rho_0^\uparrow = \rho_0^\downarrow$ and presuming that n and m are integers. The simplest choice would then be to drop the SITs and the $f_{xc}^{\uparrow,\downarrow}$ terms and to set $n = 0$, but the simplest choice is not always the best choice. *We will show in Sec. 4 that the diagrammatic analysis sometimes provides a guide as to how best to make our educated guesses.*

3 Computational Details

Calculations were done with DEMON2K [18]. Historically DEMON (*densité de Montréal*, so called because it was developed at the *Université de Montréal*) was one of the first DFT programs to use gaussian-type orbitals (GTOs) and so to be able to profit from many well-established quantum chemistry algorithms. In addition, an auxiliary basis set is used to reduce the formal scaling of the program from $\mathcal{O}(N^4)$ (because of 4-center integrals) to $\mathcal{O}(N^3)$. Prescreening and other techniques further increase the efficiency of the program. The FOCK keyword in DEMON2K provides an auxiliary-function calculation of HF exchange so that we also have access to a good approximation to Hartree-Fock and to hybrid functionals. The calculations reported here were begun at the 7th African School on Electronic Structure Methods and Applications (ASESMA) [19] with the intent of showing that research quality work could be done with limited computational resources provided one has a very good understanding of the underlying formal theory. We used a freely downloadable version of DEMON2K that runs on all the LINUX systems that we have tried. This may be used for teaching purposes as a first workbook has been written with this exactly this in mind [20, 21]. The calculations reported here were done on our portable computers.

GTO

All calculations used a valence double zeta plus polarization (DZVP) orbital basis set and the GEN-A2 auxiliary basis set. Only two functionals were used, namely the local (spin) density approximation (LDA) using the Vosko-Wilk-Nusair (VWN) parameterization [22] of Ceperley and Alder’s quantum Monte Carlo results [23] for the homogeneous electron gas [confusingly denoted VWN5 in the popular *Gaussian* program where VWN is (mistakenly) used to designate a parameterization of random-phase approximation (RPA) results in the Vosko-Wilk-Nusair article [22]].

LDA,
VWN

RPA

Our MSM-HF and MSM-VWN calculations consisted of a two-step procedure. In the first step, a reference state was imposed using the keyword MOMODIFY which allows the fixing of the occupation numbers of specific orbitals. As we wished to avoid problems with symmetry breaking in this part of the calculation, we used a high quality grid (GRID FIXED REFERENCE) and tight self-consistent field (SCF) convergence (SCFTYPE UKS TOL=1.E-8). In addition, we imposed the same occupation numbers for both spin up and spin down molecular orbitals (MOs), also with a view towards avoiding problems due to symmetry breaking. Even so, we had difficulties with symmetry breaking in our O₂ calculations and so decided to use HF reference state MOs for this molecule. The MSM-DFT concept of a reference state is a little bit like the concept of *state-averaging* in complete active space (CAS) SCF calculations in that it will impose the use of the same orbitals for all our MSM-DFT states. We set $n_\uparrow = n_\downarrow = 1/2$ within the two-orbital active space and otherwise $n = 1$ for occupied orbitals or $n = 0$ for unoccupied orbitals in all our examples. This first step of the calculations generated restart files that were then used in the second step of the calculations. Calculations in the second step read the restart files generated in the first step and calculate the energy with different orbital occupations *without* any SCF iterations (SCFTYPE UKS MAX=0). MO occupations are controlled with the MOMODIFY

SCF

MO

CASSCF

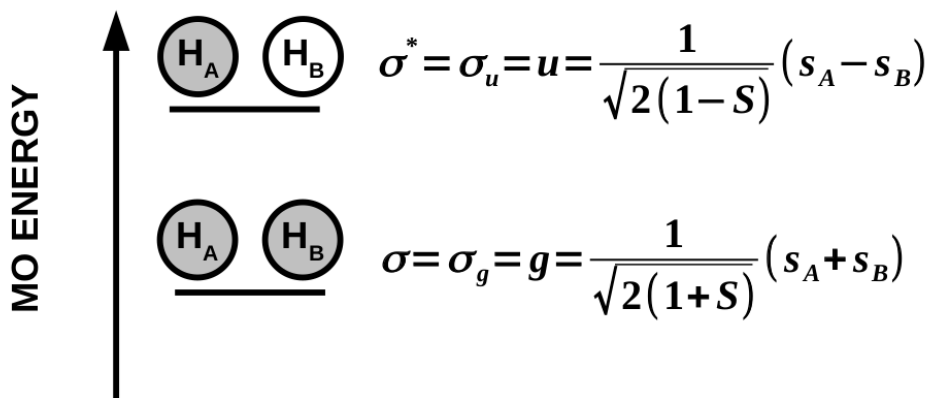


Figure 13: Textbook-like MO diagram for H_2 defining the notation used in this article. In particular, g stands for the German word *gerade* for even symmetry with respect to exchanging the A and B labels while u stands for the German word *ungerade* for odd symmetry with respect to exchanging the A and B labels. Also $S = \langle g|u \rangle$ is the overlap integral. We assume real orbitals.

keyword.

4 Exploratory Examples

The diagrammatic MSM-DFT analysis introduced in Section 2 reduces to the corresponding WFT diagrams under the EXAN, and the EXAN also places some constraints on how we are allowed to add new terms to MSM-DFT, other than those imposed by symmetry. However the EXAN does not provide a unique recipe for determining MSM-DFT terms in the absence of symmetry. In this section, we will use some specific physical examples to which we may apply the TOTEM model developed in Sec. 2 to illustrate these points. These are the two cases of H_2 and O_2 . The case of LiH is treated in the SI.

We will carry out both MSM-HF (really MSM-FOCK) and MSM-DFT (meaning MSM-VWN) calculations and compare the results against those from high-quality reference work which we will denote as EXACT. Of course, the EXACT calculations are not perfectly exact, but they are much closer to exact results than our our MSM calculations that they make an excellent comparison. These objective of these first calculations is a reality check and review of the MSM but is not really anything new. But we then go on to use the power of diagrammatic MSM to make intelligent guesses as to the value of matrix elements *not* determined by symmetry or determined by symmetry but which the diagrammatic approach tells us might be approximated in an alternative way. This is new and is intended to show the power of the the diagrammatic analysis as an analytic tool.

EXACT

4.1 H_2

H_2 is the “fruitfly” of quantum chemistry in so far as it is the simplest molecule (after H_2^+) and so is often used to illustrate various level of theory. We will not be different in this respect. **Figure 13** shows the usual linear combination of (valence) atomic orbitals

LCAO

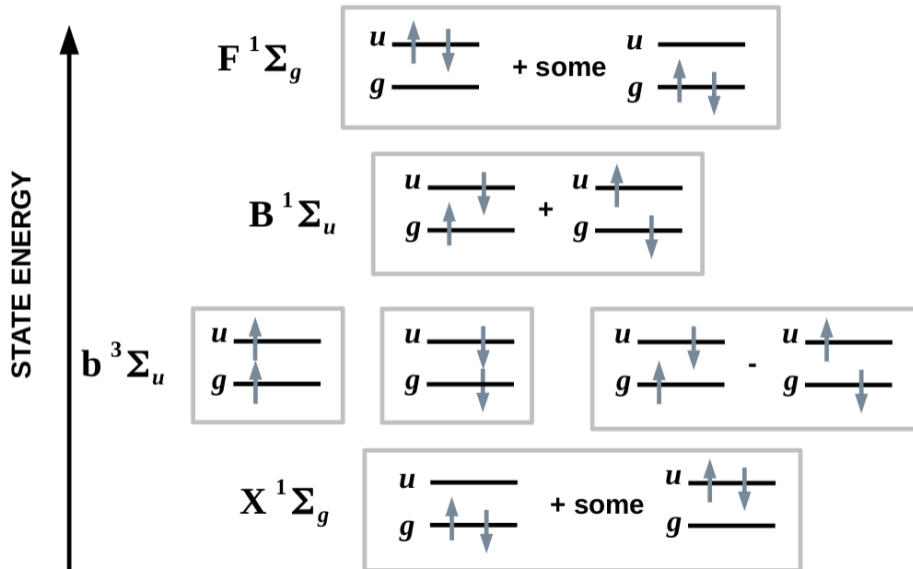


Figure 14: Diagram showing the six states which may be constructed by placing two electrons in the two MOs of Fig. 13.

(LCAO) description usually used as a first approximation for describing the MOs of H_2 and is primarily shown as a quick way to introduce our notation. This is a TOTEM identical to that introduced in Fig. 2, except that i has been replaced by g and a has been replaced by u so that there is additional symmetry. This gives rise to four states, namely the ground $X^1\Sigma_g^+$ state, the $b^3\Sigma_u^+$ triplet state, the $B^1\Sigma_g^+$ open-shell singlet state, and the $F^1\Sigma_g^+$ doubly-excited singlet state (**Fig. 14**). We will habitually drop the "+" part of the symmetry label as it is not important in the present context.

The 1971 review written by Sharp provides a nice picture of what was known about the various potential energy curves (PECs) of H_2 and its ions at that time [25]. Our TOTEM can only hope to describe some of these states, namely the EXACT PECs shown in **Fig. 15**. These are PECs from the well-known excellent calculations of Kołos and Wolniewicz obtained using explicit $r_{1,2}$ basis functions [26, 27, 28, 29, 30, 31, 32, 33, 34, 35]. In practice we use numbers obtained by digitizing Fig. 1 of Ref. [36] which provides curves which are already much more accurate than what we expect from our MS-DFT calculations. Note that the $E, F^1\Sigma_g$ curve has a double minimum arising from an avoided crossing between the $E^1\Sigma_g(1\sigma_g, 2\sigma_g)$ diabatic curve (left-hand minimum) and the $F^1\Sigma_g(1\sigma_u^2)$ (right-hand minimum).

PEC

Our MSM-HF and MSM-VWN calculations use a reference calculation whose PEC is shown in **Fig. 16** as a function of the bond distance R . Here, and throughout this subsection, we plot the H_2 energy relative to twice the energy of a single neutral hydrogen atom calculated using identical conditions (atomic basis set, density fitting, basis set, grid, convergence conditions) to those used in calculating the H_2 molecule reference state. It is evident that the MSM-VWN PEC is much lower in energy than the MSM-HF PEC although, as **Fig. 17** shows, the difference in the corresponding HF and VWN MO energy curves is much less dramatic. Notable in the figure is that the u MO energy is unbound in HF for bond lengths below about $R \approx 1.6$ bohr and in HF for bond lengths below

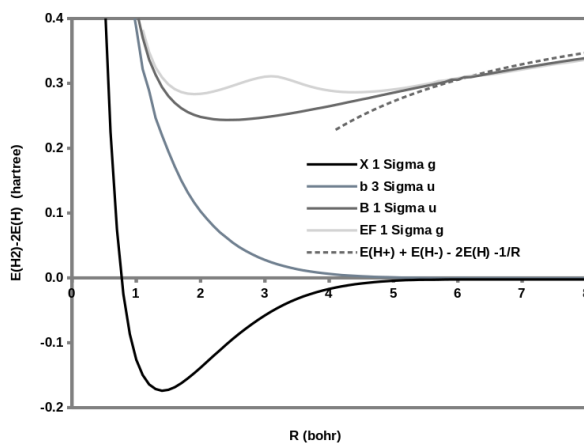


Figure 15: EXACT H_2 PECs obtained by Kołos and Wolniewicz by calculations using basis functions with an explicit $r_{1,2}$ dependence. See text. We used the value of 0.754189 eV for the electron affinity of the hydrogen atom determined by laser photoelectron spectroscopy [24] to construct the dashed asymptotic estimate for the long distance asymptote in the $[H^+ H^- \leftrightarrow H^- + H^+]$ limit.

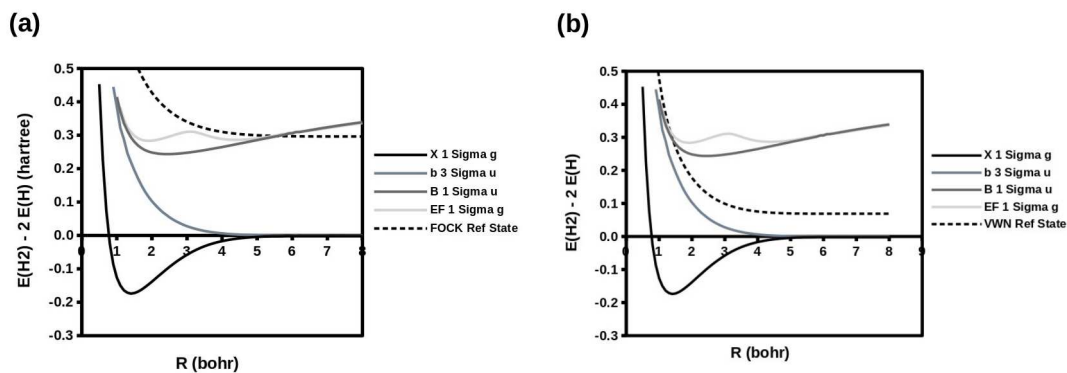


Figure 16: MSM reference state PECs: (a) MSM-HF and (b) MSM-VWN. The energies of the separated atoms have been calculated as twice the energy of the neutral hydrogen atom calculated using identical conditions (atomic basis set, density fitting, basis set, grid, convergence conditions) to those used in calculating the H_2 molecule reference state.

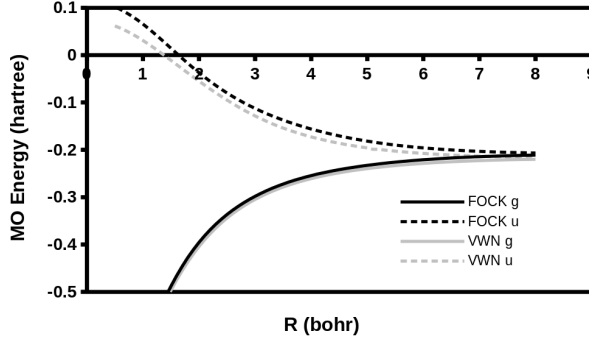


Figure 17: MO energies from the HF and VWN reference state calculations.

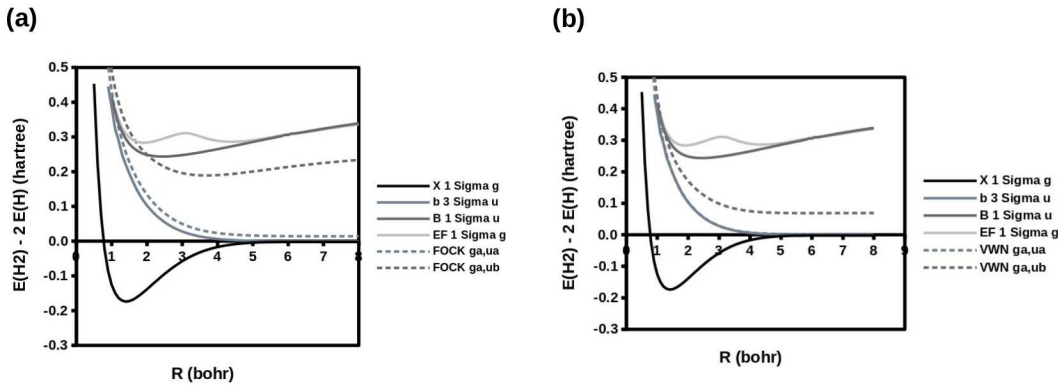


Figure 18: HF and VWN PECs for the triplet state determinant $\Psi_{1,1} = |g, u\rangle$ and for the mixed-symmetry singly-excited determinant $\Psi_M = |g, \bar{u}\rangle$. Note that the VWN triplet PEC is indistinguishable from the EXACT triplet PEC.

$R \approx 1.3$ bohr so that the reference state cannot be considered to be converged with respect to basis set expansion at short bond lengths. This is an obvious difficulty with the MSM, but is not very important in the present application.

The first thing that needs to be done in the MSM is to calculate the energies corresponding to a pure-symmetry triplet determinant $\Psi_{S,M} = \Psi_{1,\pm 1}$ and for a mixed-symmetry singly-excited determinant Ψ_M . We have chosen to do this for $\Psi_{1,1} = |g, u\rangle$ and for $\Psi_M = |g, \bar{u}\rangle$. The results are shown in **Fig. 18**. Note that we are using the unrelaxed orbitals from the reference calculation to evaluate the single determinant energies. Only the spin-orbital occupations have been changed using the `MOMODIFY` keyword. Relaxing the triplet HF orbitals would lower the HF triplet PEC, bringing it closer to the EXACT triplet PEC. Interestingly the VWN triplet PEC is indistinguishable from the EXACT triplet PEC. The HF mixed-symmetry PEC is not only higher in energy and closer to the EXACT $B^1\Sigma_u$ PEC than is the VWN mixed-symmetry PEC, but the HF mixed-symmetry PEC has a minimum. This is similar to the EXACT $B^1\Sigma_u$ PEC but is lacking in the VWN mixed-symmetry PEC. This is a first indication of a failure of the MSM-VWN calculation to produce a qualitatively correct result.

According to the explanation given in Section 2, these VWN single-determinant energies constitute a way to include dynamical correlation in the diagonal elements of the CI

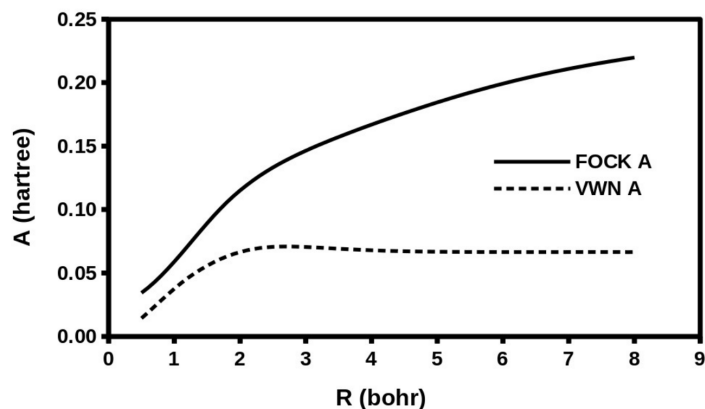


Figure 19: MSM $A = E[|g, \bar{u}|] - E[|g, u|]$ matrix element.

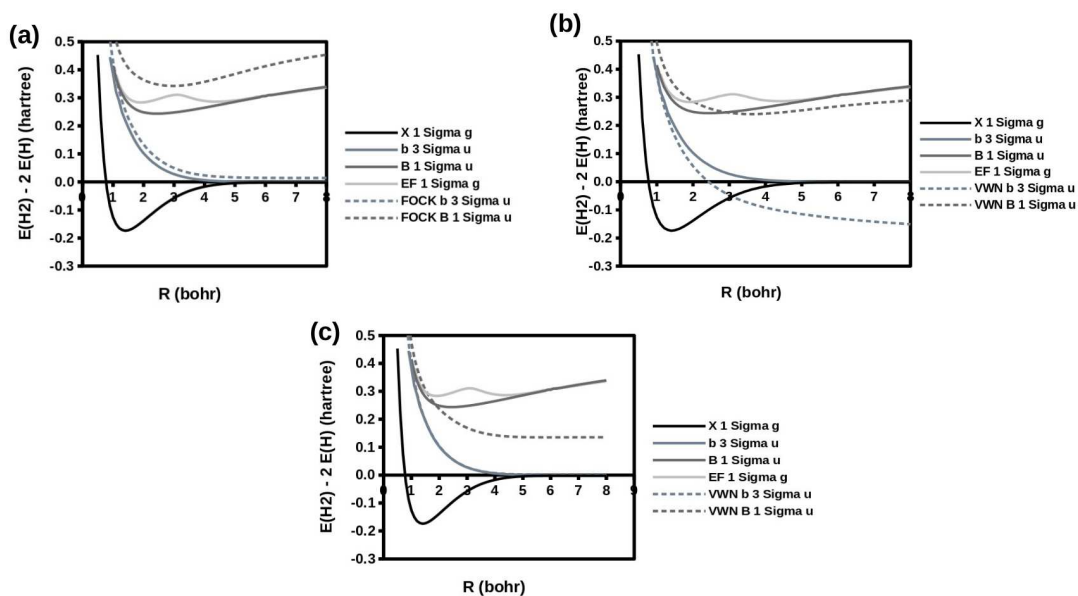


Figure 20: Three ways to calculate MSM $b^3\Sigma_u$ and $B^1\Sigma_u$ PECs: (a) MSM-HF, (b) MSM-VWN using HF A , and (c) MSM-VWN (using VWN A).

eigenvalue problem,

$$\begin{bmatrix} E[|u, \bar{g}\rangle] & A \\ A & E[|g, \bar{u}\rangle] \end{bmatrix} \begin{pmatrix} C_g^u \\ C_{\bar{g}}^u \end{pmatrix} = E \begin{pmatrix} C_g^u \\ C_{\bar{g}}^u \end{pmatrix}. \quad (12)$$

The problem then is to introduce static correlation by choosing an appropriate value of the matrix element A . The default guess is to use WFT methods to obtain,

$$A^{\text{HF}} = E_{\text{HF}}[|g, \bar{u}\rangle] - E_{\text{HF}}[|g, u\rangle] = (gu|f_H|ug). \quad (13)$$

This matrix element is shown in **Fig. 19** as a function of distance. This gives the MSM results shown in **Fig. 20**. By construction, the MSM-HF $b^3\Sigma_u$ state made by subtracting A from the energy of the mixed symmetry state has exactly the same energy as the HF $b^3\Sigma_u$ state shown in Fig. 18. The MSM-HF $B^3\Sigma_u$ PEC is a significant overestimate of the EXACT $B^3\Sigma_u$ PEC compared to what is obtained from the mixed-state PEC (Fig. 18) which matches the EXACT PEC remarkably well for $R \leq 2$ bohr. However the MSM-HF $B^3\Sigma_u$ PEC, though overestimating the energy, is clearly a better global description as it has a very similar overall shape to the corresponding EXACT PEC including having a minimum in about the right place. This state should also dissociate into the ions whose energy, relative to the neutral atoms, is 0.57 hartree in our HF calculations.

Figure 20 confirms that using the HF A matrix element in the MSM-VWN calculation by subtracting A from the energy of the mixed symmetry state gives a very different energy than that obtained from calculating the energies of the two single determinantal $\Psi_{1,\pm 1}$ triplet states. In particular, the dissociation limit of the MSM-VWN $B^1\Sigma_u$ PEC is disastrously low. On the other hand, the MSM-VWN $B^1\Sigma_u$ PEC obtained in this way is (arguably) not that bad. Its energy is about right and it has a minimum, just like the EXACT $B^1\Sigma_u$ PEC.

In order to fix the MSM-VWN triplet state problem, we must reset the A matrix element to be,

$$A^{\text{VWN}} = E_{\text{VWN}}[|g, \bar{u}\rangle] - E_{\text{VWN}}[|g, u\rangle] \approx (gg|f_{xc}^{\uparrow,\downarrow} - f_{xc}^{\downarrow,\uparrow}|uu). \quad (14)$$

This gives the PECs in part (c) of Fig. 20 where all the MSM-VWN triplet curves are now perfectly degenerate by construction. The MSM-VWN $B^1\Sigma_u$ PEC matches the EXACT $B^1\Sigma_u$ PEC for $R \leq 2$ bohr, but thereafter is a significant underestimate of the EXACT PEC. This correlates very nicely with the fact that the VWN and HF values of A are roughly similar for $R \leq 2$ bohr. Beyond this bond length, the HF A increases while the VWN A levels out to a near constant value of about 0.066 hartree. Perhaps surprisingly, the MSM-VWN $B^1\Sigma_u$ PEC is dissociating to an energy of about 0.135 hartree which is well below the expected VWN ionic dissociation energy of 0.515 hartree. This strange result has been seen before where it was also noted that a qualitatively correct $B^1\Sigma_u$ PEC is obtained using TD-DFT in the Tamm-Dancoff approximation (TDA) [37]. The corresponding A matrix element in TDA TD-DFT is

$$A^{\text{TDA TD-DFT}} = (gu|f_H|ug) + (gg|f_{xc}^{\uparrow,\downarrow}|uu), \quad (15)$$

represented diagrammatically in **Fig. 21**. This might suggest the superiority of TDA TD-DFT over MS-DFT, but it should be noted that the two theories give very similar results at the ground-state equilibrium bond length of about 1.4 bohr, where the hypothesis of a single-determinantal ground state wave function remains reasonable.

TDA

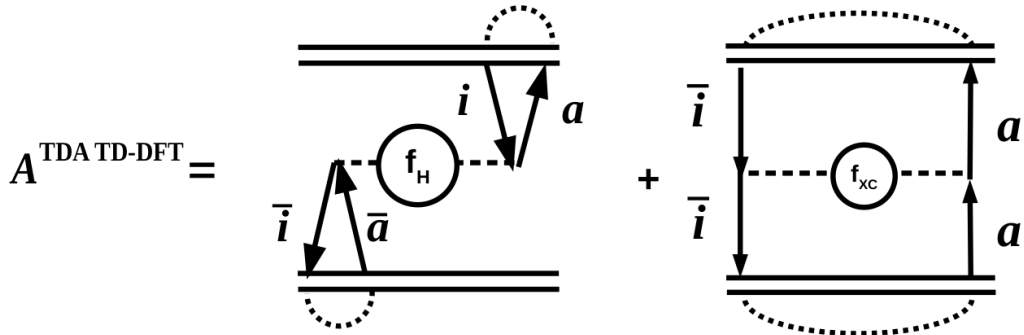


Figure 21: Diagrammatic representation of the A matrix element in TDA TD-DFT. The indices i and a have been used to facilitate comparison with Figs. 30 and 11. For H_2 , replace i with g and a with u .

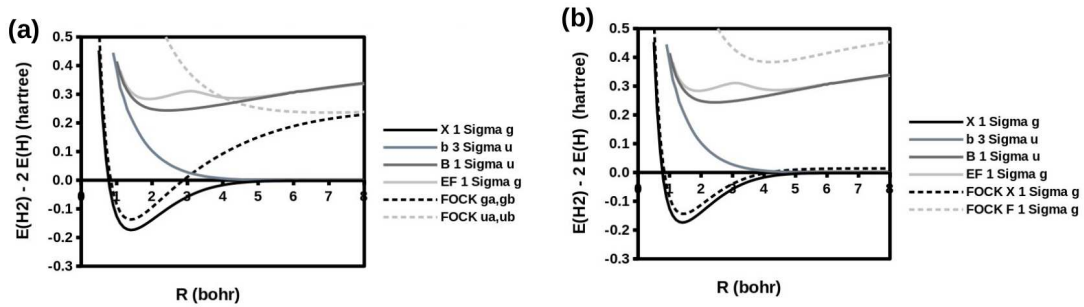


Figure 22: $X^1\Sigma_g$ and $F^1\Sigma_g$ HF PECs: (a) without A and (b) including A .

Up to this point, there is nothing (or at least very little) that is new. We have simply illustrated the use of MS-DFT for describing the triplet and open-shell singlet PECs of H_2 . However, *we now look at something new* inspired by diagrammatic MS-DFT. Let us begin with WFT. **Figure 22(a)** shows the ground and doubly-excited state PECs calculated within the single-determinantal approximation. These two HF PECs are dissociating to the same wrong energy. The reason that this happens is well understood but may require review for some readers as it is closely associated with the valence-bond (VB) method which allows wave functions to be interpreted in terms of Lewis dot structures (LDSs) and which is not as often taught as it once was [38]. At large R , the overlap matrix (Fig. 13) goes to zero and the limiting form of the MOs is just,

$$\begin{aligned} g &= \frac{1}{\sqrt{2}}(s_A - s_B) \\ u &= \frac{1}{\sqrt{2}}(s_A + s_B). \end{aligned} \quad (16)$$

This allows us to calculate the large R limit for the three triplet $b^3\Sigma_u$ wave functions $\Psi_{S,M}$,

$$\begin{aligned} \Psi_{1,1} &= |g, u| \\ &\rightarrow -|s_A, s_B| \\ &\quad [H\uparrow H\uparrow] \\ \Psi_{1,0} &= \frac{1}{\sqrt{2}}(|g, \bar{u}| - |u, \bar{g}|) \\ &\rightarrow -\frac{1}{\sqrt{2}}(|s_A, \bar{s}_B| - |s_B, \bar{s}_A|) \\ &\quad [H\uparrow H\downarrow \leftrightarrow H\downarrow H\uparrow] \\ \Psi_{1,-1} &= |\bar{g}, \bar{u}| \\ &\rightarrow |\bar{s}_A, \bar{s}_B| \\ &\quad [H\downarrow H\downarrow], \end{aligned} \quad (17)$$

where the corresponding LDSs are also shown. This explains why the $b^3\Sigma_u$ PEC dissociates to the neutral atom limit in Fig. 15. Similarly for the open-shell singlet $B^1\Sigma_u$ wave function,

$$\begin{aligned} \Psi_{0,0} &= \frac{1}{\sqrt{2}}(|g, \bar{u}| + |u, \bar{g}|) \\ &\rightarrow \frac{1}{\sqrt{2}}(|s_A, \bar{s}_A| - |s_B, \bar{s}_B|) \\ &\quad [H:^- H^+ \leftrightarrow H^+ H^-], \end{aligned} \quad (18)$$

which explains why the $B^1\Sigma_u$ PEC dissociates to the separated ion limit in Fig. 15. However,

$$\begin{aligned} |g, \bar{g}| &\rightarrow \frac{1}{\sqrt{2}} \left[\frac{1}{\sqrt{2}}(|s_A, \bar{s}_A| + |s_B, \bar{s}_B|) + \frac{1}{\sqrt{2}}(|s_A, \bar{s}_B| + |s_B, \bar{s}_A|) \right] \\ &\quad [H:^- H^+ \leftrightarrow H^+ H^-] + [H\uparrow H\downarrow \leftrightarrow H\downarrow H\uparrow] \\ |u, \bar{u}| &\rightarrow \frac{1}{\sqrt{2}} \left[\frac{1}{\sqrt{2}}(|s_A, \bar{s}_A| + |s_B, \bar{s}_B|) + \frac{1}{\sqrt{2}}(|s_A, \bar{s}_B| + |s_B, \bar{s}_A|) \right] \\ &\quad [H:^- H^+ \leftrightarrow H^+ H^-] + [H\uparrow H\downarrow \leftrightarrow H\downarrow H\uparrow], \end{aligned} \quad (19)$$

which shows that the ground and doubly-excited determinants dissociate to the same incorrect limit which is a combination of ionic and of neutral atom separation. In the large R limit, the $X^1\Sigma_g$ wave function should have the form,

$$\frac{1}{\sqrt{2}} (|g, \bar{g}\rangle - |u, \bar{u}\rangle) = \frac{1}{\sqrt{2}} (|s_A, \bar{s}_B\rangle + |s_B, \bar{s}_A\rangle) \\ [\text{H}\uparrow \text{H}\downarrow \leftrightarrow \text{H}\downarrow \text{H}\uparrow], \quad (20)$$

and the $F^1\Sigma_g$ wave function should have the form,

$$\frac{1}{\sqrt{2}} (|g, \bar{g}\rangle + |u, \bar{u}\rangle) = \frac{1}{\sqrt{2}} (|s_A, \bar{s}_B\rangle - |s_B, \bar{s}_A\rangle) \\ [\text{H}:\text{H}^+ \leftrightarrow \text{H}^+ \text{H}:\text{H}^-]. \quad (21)$$

For smaller values of R , the first approximation is that these two wave functions have the form,

$$\Psi = C_0 |g, \bar{g}\rangle + C_{g, \bar{g}}^{u, \bar{u}} |u, \bar{u}\rangle, \quad (22)$$

and the coefficients and corresponding energies are determined by solving the small CI problem,

$$\begin{bmatrix} E[|g, \bar{g}\rangle] & B \\ B & E[|u, \bar{u}\rangle] \end{bmatrix} \begin{pmatrix} C_0 \\ C_{g, \bar{g}}^{u, \bar{u}} \end{pmatrix} = E \begin{pmatrix} C_0 \\ C_{g, \bar{g}}^{u, \bar{u}} \end{pmatrix}. \quad (23)$$

This is reminiscent of Eq. [12], except that the two diagonal elements are no longer equal, so that simple quadratic equation must be solved to find the eigenvalues. **Figure 23** shows that

$$B = (ug | f_H | ug), \quad (24)$$

which is the same as the A matrix element already calculated as long as the MOs are real. Solving the CI Eq. [23], gives the graph shown in part (b) of Fig. 22. Not only does the $X^1\Sigma_g$ PEC dissociate correctly to the limit of separated neutral atoms (within the accuracy of the frozen reference orbital approximation being used) but the $F^1\Sigma_g$ PEC has a minimum around the right hand minimum of the $E, F^1\Sigma_g$ PEC as it should and dissociates correctly towards the HF ionic limit of 0.57 hartree.

The situation is very different in DFT. When the exact xc functional is used, there is no NVR problem and a single-determinantal wavefunction suffices. This is easily shown by setting the g orbital equal to the square root of half the exact charge density and then reconstructing the non-interacting potential as,

$$\left(-\frac{1}{2} \nabla^2 + v_s \right) \psi_g = \epsilon_g \psi_g \\ \psi_g = \epsilon_g + \frac{1}{2} \nabla^2 \psi_g. \quad (25)$$

That ψ_g is the ground state for this v_s results from the absence of nodes in ψ_g . However practical xc approximations result in symmetry breaking beyond the Coulson-Fischer point (e.g., see Ref. [37] and references therein) where the different-orbitals-for-different-spins (DODS) solution becomes lower in energy than the same-orbitals-for-different-spins (SODS) solution. This implies the need to improve the wave function by taking a linear combination of two determinants as in Eq. [22]. Alternatively, allowing the symmetry

DODS
SODS

$$B^{\text{HF}} = \langle \Phi | \hat{H} | \Phi_{i, \bar{i}}^{a, \bar{a}} \rangle =$$

Figure 23: Diagrammatic evaluation of $B^{\text{HF}} = \langle \Phi | \hat{H} | \Phi_{i, \bar{i}}^{a, \bar{a}} \rangle$. In the particular case of H_2 , then i and a should be replaced respectively with g and u .

breaking to occur and using the DODS solution suffices for many cases, but *not* when excited states are to be calculated from the ground state solution (e.g., Ref. [16]) as symmetry is needed to get even qualitatively correct PECs. It is therefore important to be able to formulate a multideterminantal DFT, using WFT to include static correlation and DFT to include static correlation and trusting that overcounting of correlation effects will not pose a serious problem in practical applications as long as the number of determinants used in the multideterminantal DFT is kept small.

Inspired by MSM-DFT, we will use DFT to calculate the diagonal elements in the CI Eq. [23]. But what shall we use for B ? Unlike in MSM-DFT we have no symmetry to guide us! The two “obvious” choices for B are either to use the HF A from WFT or to use the VWN A obtained from MSM-DFT using symmetry and for a different purpose. **Figure 24** shows the results of these two choices. The choice of using the HF $B = A$ to correct the single-determinantal VWN energies looks like it might be reasonable for the $F^1\Sigma_g$ excited state, but it is clearly wrong for the very important problem of obtaining the correct dissociation of the $X^1\Sigma_g$ ground state. If B may be replaced with A in WFT, we might also suppose based upon diagrammatic MS-DFT that B might also be replaced with A in DFT, provided we use the correct MS-DFT A . Remarkably Fig. 24(c) shows that this is exactly correct for obtaining the correct dissociation of the ground state. *It is worth emphasizing that this an apparently new result based upon an educated guess obtained from our diagrammatic analysis of MS-DFT. If this holds in a more general context, then we shall have produced something new and unexpected—namely a parameter-free multideterminantal DFT for ground state potential energy surfaces.* The corresponding $F^1\Sigma_g$ PEC is less impressive, suggesting that we should use an alternative route to obtain this excited-state PEC, such as doing response theory on our new multideterminantal DFT ground state energy expression (something whose details should not be too difficult to work out.) However the $F^1\Sigma_g$ and $B^1\Sigma_u$ PECs *are* fully consistent in that they are both converging to the same value of about 0.135 hartree, instead of the expected DFT value of 0.514 hartree for dissociation into separated ions. Alternatively, we might say that the ionic dissociation energy is 0.135 hartree in this model and everything at least

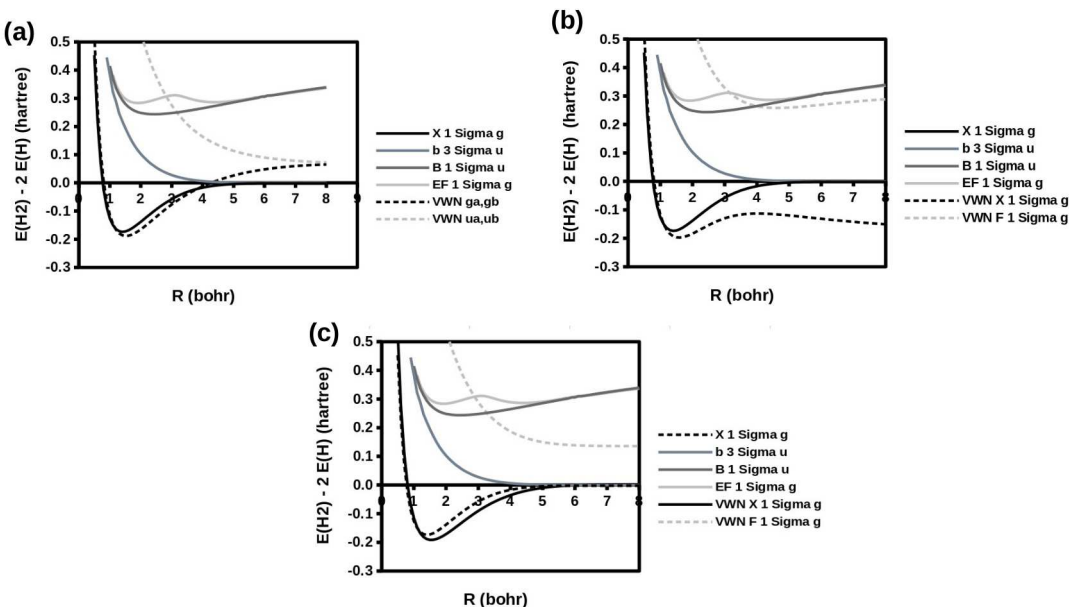


Figure 24: Three ways to calculate MSM $X\ ^1\Sigma_g$ and $F\ ^1\Sigma_g$ PECs: (a) VWN single-determinantal energies, (b) VWN single-determinantal energies corrected using the HF $B = A$, and (c) VWN single-determinantal energies obtained using $B = \text{VWN } A$.

seems to be internally consistent.

4.2 LiH

The example of LiH is treated in the SI.

4.3 O₂

Our third and last example of applying MSM-DFT is to O₂. Our specific interest is in reactions of singlet O₂ (¹O₂) with molecules such as the classic photochemical synthesis of the anthelmintic drug ascaridole from α -terpene and ¹O₂ [39, 40, 41, 42, 43]. The presence of α -terpene will necessarily lower the symmetry of the system making ordinary MSM-DFT difficult, hence our desire to use diagrammatic MSM-DFT to seek alternative approximations which might ultimately free us from the symmetry-dependence of classic MSM-DFT.

A research spin-off [16] of a relatively new pedagogical workbook [21] presents one of the few, and certainly the most thorough, applications of MSM-DFT to the spin- and spacial-symmetry multiplet splitting problem in O₂. We will only summarize the highlights here and then move on to a diagrammatic analysis.

A textbook-like representation of the key frontier MOs is shown in **Fig. 25**. Note that we are going to be lazy and just abbreviate the $\pi_x^* = \pi_g^x$ and $\pi_y^* = \pi_g^y$ MOs as x and y respectively. As shown in Ref. [16], a TOTEM may be constructed with the states shown in **Fig. 26**. The appearance of this diagram depends upon whether real or complex MOs are used [16]. We are using real-valued MOs. It is evident that this state diagram looks very different from those shown previously (Figs. 2, 14, and 28). This can cause problems

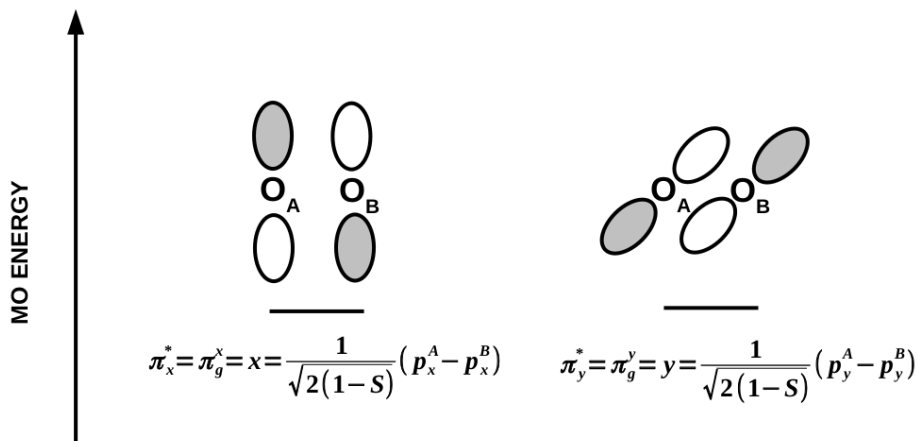


Figure 25: Textbook-like MO diagram for O_2 . This molecule is different from either H_2 or LiH because the MOs are energetically degenerate. The orbitals have been chosen to be real valued and $S = \langle p_x^A | p_x^B \rangle = \langle p_y^A | p_y^B \rangle$ is the overlap integral. Note the drastic abbreviations $\pi_x^* \rightarrow x$ and $\pi_y^* \rightarrow y$. [*Gerade* (g) and *ungerade* (u) refer to inversion through the center of symmetry.]

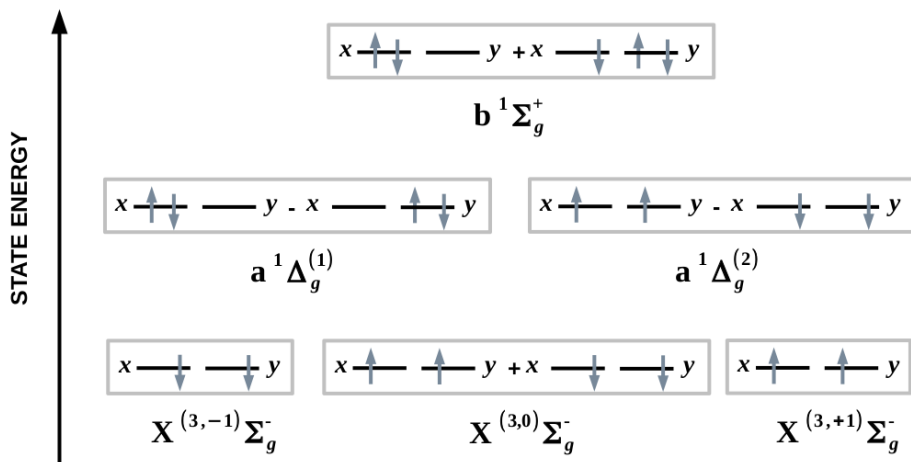


Figure 26: Diagram showing the six states which may be constructed by placing two electrons in the two MOs of Fig. 25.

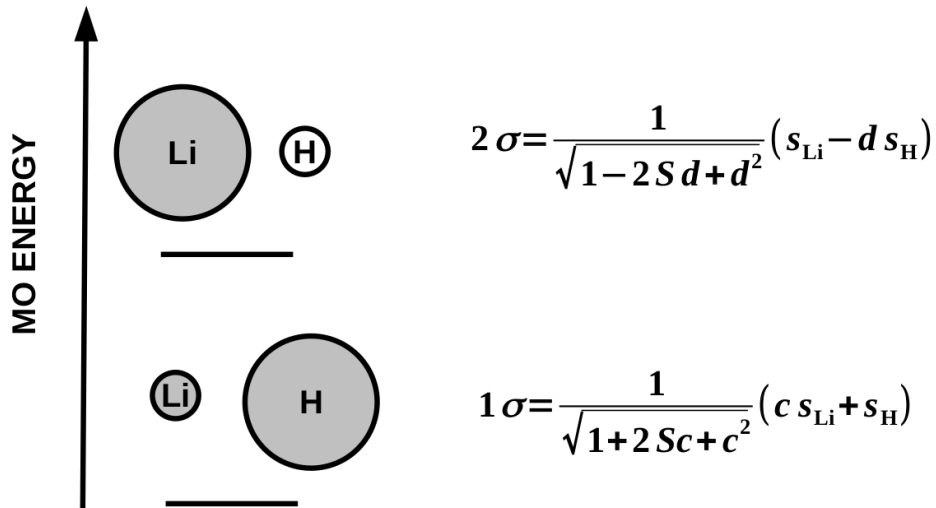


Figure 27: Textbook-like MO diagram for LiH. There is only axial symmetry in this molecule, so the valence MOs are labeled as 1σ and 2σ . Orthonormality fixes $d = (S + c)/(1 + Sc)$ where $S = \langle s_{\text{Li}} | s_{\text{H}} \rangle$ is the overlap integral.

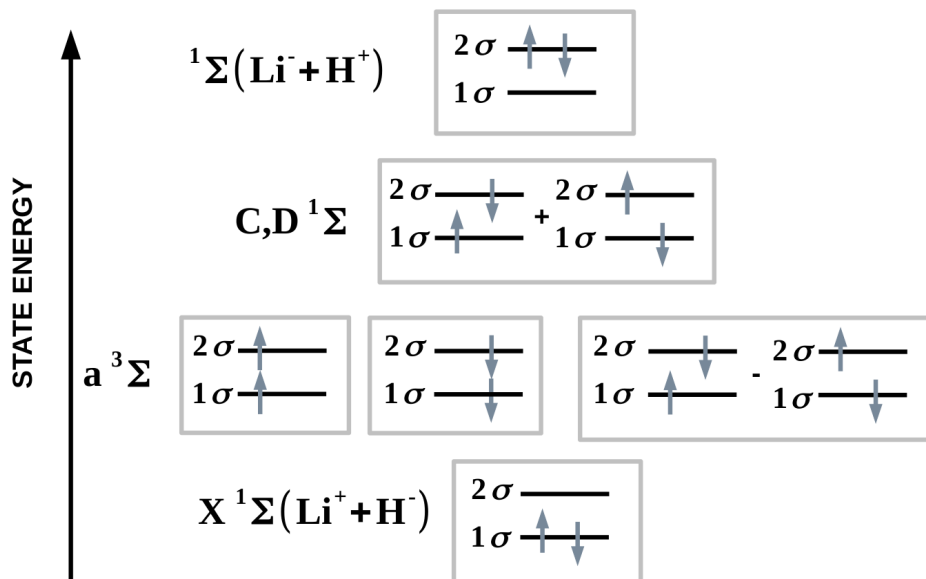


Figure 28: Diagram showing the six states which may be constructed by placing two electrons in the two MOs of Fig. 27.

when using diagrammatic theory. On the other hand, the $X^{(3,0)\Sigma_g^-}$ and $a^1\Delta_g^{(2)}$ states form a natural \pm pair, perfect for MSM, as do the $a^1\Delta_g^{(1)}$ and $b^1\Sigma_g^+$ states. We may then easily work out that,

$$\begin{aligned} E[X^3\Sigma_g^-] &= E[|x, y\rangle] \\ E[a^1\Delta_g] &= E[|x, y\rangle] + 2F \\ E[b^1\Sigma_g^+] &= E[|x, y\rangle] + 2P, \end{aligned} \quad (26)$$

where the spin-flip energy,

$$F = E[|x, \bar{y}\rangle] - E[|x, y\rangle] \quad (27)$$

and the spin-pairing energy,

$$P = E[|x, \bar{x}\rangle] - E[|x, \bar{y}\rangle]. \quad (28)$$

The $M_S = 0$ part of the MSM CI matrix is,

$$\mathbf{H} = \begin{bmatrix} E[|x, \bar{y}\rangle] & A & 0 & 0 \\ A & E[|y, \bar{x}\rangle] & 0 & 0 \\ 0 & 0 & E[|x, \bar{x}\rangle] & B \\ 0 & 0 & B & E[|y, \bar{y}\rangle] \end{bmatrix}, \quad (29)$$

where Brillouin's theorem has been used to zero out some of the matrix elements. Clearly $E[|x, \bar{y}\rangle] = E[|y, \bar{x}\rangle]$ and $E[|x, \bar{x}\rangle] = E[|y, \bar{y}\rangle]$ for the isolated molecule. Comparing Eqs. (26)-(30) shows that,

$$\begin{aligned} A &= F = E[|x, \bar{y}\rangle] - E[|x, y\rangle] \\ B &= P - F = E[|x, \bar{x}\rangle] + E[|x, y\rangle] - 2E[|x, \bar{y}\rangle]. \end{aligned} \quad (30)$$

While the expression for the A matrix element is familiar, we have never before had an MSM expression for the B matrix element, though $B = A$ seemed to be an excellent educated guess in H_2 . Indeed the DFT-MSM results given in Ref. [16] suggest that $B = A$ is probably a pretty reasonable guess! This is the point that we wish now to explore.

We will use the diagrammatic analysis as a tool to aid us. The price that we pay for this is that, although the results will be independent of the choice of physical vacuum, the appearance of the diagrams (e.g., which are direct and which are exchange diagrams) depends upon the choice of the reference. In order to be as consistent as possible with everything that has been done up to this point, we will choose $\Phi = |x, \bar{x}\rangle$ as the physical vacuum. In WFT (either by direct evaluation or by MSM-HF), the diagrams of A are shown in Fig. 30 when i and a are replaced respectively by x and y . In either case, the matrix element evaluates to

$$A^{\text{HF}} = (xy|f_H|yx). \quad (31)$$

However the situation is more complex for the B matrix element. The diagram for direct evaluation of B is identical to that of A (Fig. 23 when i and a are replaced respectively by x and y),

$$B^{\text{HF}} = (xy|f_H|yx). \quad (32)$$

$$B^{\text{HF-MSM}} = \langle \Phi | \bar{H} | \Phi \rangle + \langle \Phi_x^y | \hat{H} | \Phi_x^y \rangle - 2 \langle \Phi_x^y | \hat{H} | \Phi_x^y \rangle =$$

$$2(xx|f_H|xx) \quad -2(xx|f_H|yy) \quad -(xx|f_H|xx) \quad +(xy|f_H|yx)$$

$$+(xx|f_H|yy) \quad -2(xy|f_H|yx)$$

Figure 29: Diagrammatic development of the MSM-HF expression for B in O_2 . Note that many terms have been canceled including terms with different spins but the same algebraic expressions.

$$A^{\text{HF}} = \langle \Phi_i^a | \hat{H} | \Phi_i^{\bar{a}} \rangle =$$

Figure 30: Diagrammatic evaluation of $A^{\text{HF}} = \langle \Phi_i^a | \hat{H} | \Phi_i^{\bar{a}} \rangle$.

(a)

$$B^{\text{DFT-MSM}} = E[\Phi] + E[\Phi_{\bar{x}}^y] - 2E[\Phi_{\bar{x}}^{\bar{y}}] =$$

$$\begin{aligned}
& - 2(xx|f_H|xx) \quad - 2(xx|f_H|yy) \quad + \int v_{xc}^{\uparrow} \rho_x \quad - \int v_{xc}^{\uparrow} \rho_y \\
& + (xx|f_H|yy) \quad + 2(xx|f_{xc}^{\uparrow, \uparrow}|yy) \quad - (xx|f_{xc}^{\uparrow, \downarrow}|yy) \quad + \text{SITs}
\end{aligned}$$

(b)

$$\begin{aligned}
\text{SITs} = & - \frac{1}{2} (xx|f_{xc}^{\uparrow, \uparrow}|xx) \quad - \frac{1}{2} (yy|f_{xc}^{\uparrow, \uparrow}|yy)
\end{aligned}$$

Figure 31: Diagrammatic development of the DFT-MSM expression for B in O_2 truncated to second order. Note that the xc terms are functionals of the density corresponding to the reference density with both electrons in x which we will simply denote as $[\rho_x, \rho_x]$ in the TOTEM. Also many terms have been canceled including terms with different spins but the same algebraic expressions.

On the other hand, the diagrams obtained using the MSM formula in Eq. (30) are shown in **Fig. 29** and evaluate to

$$\begin{aligned}
B^{\text{HF}} &= (xx|f_H|xx) - (xx|f_H|yy) - (xy|f_H|yx) \\
&= (xy|f_H|yx) + [(xx|f_H|xx) - (xx|f_H|yy) - 2(xy|f_H|yx)]. \quad (33)
\end{aligned}$$

Equations (32) and (33) are actually identical but the proof has been relegated to the SI as it is a little involved. In particular, it follows that $B = A$ in WFT.

Now let us turn to DFT. Traditional symmetry-based DFT-MSM arguments were used in Ref. [16] to justify the use of Eq. (33). Diagrammatic analysis of the expression gives **Fig. 31** rather than Fig. 29 for the B matrix element. Nevertheless the general pattern is consistent with the correspondance rules set out in Sec. 2. Evaluating the diagrams gives

explicitly,

$$\begin{aligned}
B^{\text{DFT-MSM}} &= 2(xx|f_H|xx) - (xx|f_H|yy) \\
&+ \int v_{xc}^\uparrow[\rho_x, \rho_x](1)\rho_x(1) d1 - \int v_{xc}^\uparrow[\rho_x, \rho_x](1)\rho_y(1) d1 \\
&+ (xx|2f_{xc}^{\uparrow,\uparrow}[\rho_x, \rho_x] - 2f_{xc}^{\uparrow,\downarrow}[\rho_x, \rho_x]|yy) \\
&- \frac{1}{2} \{ (xx|f_{xc}^{\uparrow,\uparrow}[\rho_x, \rho_x]|xx) + (yy|f_{xc}^{\uparrow,\uparrow}[\rho_x, \rho_x]|yy) \}. \quad (34)
\end{aligned}$$

This expression is a little problematic should we wish to compare it with Eqs. (32) and (33) because of the presence of terms involving $v_{xc}^\uparrow[\rho_x, \rho_x]$. We can get around this by using another expansion,

$$\begin{aligned}
\int v_{xc}^\uparrow[\rho_x, \rho_x](1)\rho_y(1) d1 &= \int v_{xc}^\uparrow[\rho_y, \rho_y](1)\rho_y(1) d1 + (xx|f_{xc}^{\uparrow,\uparrow}[\rho_y, \rho_y]|yy) - (yy|f_{xc}^{\uparrow,\uparrow}[\rho_y, \rho_y]|yy) \\
&+ (xx|f_{xc}^{\uparrow,\downarrow}[\rho_y, \rho_y]|yy) - (yy|f_{xc}^{\uparrow,\downarrow}[\rho_y, \rho_y]|yy) + \text{HOT}. \quad (35)
\end{aligned}$$

As

$$f_{xc}^{\sigma,\tau}[\rho_y, \rho_y](1, 2) = f_{xc}^{\sigma,\tau}[\rho_x, \rho_x](1, 2) + \text{HOT}, \quad (36)$$

then the final second-order expansion for the DFT-MSM B becomes,

$$\begin{aligned}
B^{\text{DFT-MSM}} &= (xx|f_H|xx) + [(xx|f_H|xx) + (xx|f_{xc}^{\uparrow,\uparrow}|xx)] \\
&- (xx|f_H|yy) \\
&+ (xx|f_{xc}^{\uparrow,\uparrow}|yy) \\
&+ [(yy|f_{xc}^{\uparrow,\downarrow}|yy) - 2(xx|f_{xc}^{\uparrow,\downarrow}|yy)] \\
&- \frac{1}{2} [(xx|f_{xc}^{\uparrow,\uparrow}|xx) + (yy|f_{xc}^{\uparrow,\uparrow}|yy)]. \quad (37)
\end{aligned}$$

Note how this fits the general form expected from applying Eq. (11) to Eq. (33).

It is also far from obvious that $B^{\text{DFT-MSM}}$ should equal,

$$A^{\text{DFT-MSM}} = (xx|f_{xc}^{\uparrow,\uparrow}|yy) - (xx|f_{xc}^{\uparrow,\downarrow}|yy), \quad (38)$$

and they are probably not equal in practice. Setting them equal to each other, and hence lifting some of the symmetry-imposed degeneracy, might be the price that we have to pay to free ourselves from symmetry in the MSM. If so, we would still like to insure that $B^{\text{DFT-MSM}} \approx A^{\text{MSM-DFT}}$. In order to investigate this further, we carried out MSM-HF and MSM-VWN calculations beginning with a reference state with half an electron of each spin in the x and y orbitals. We followed the same procedure as for H_2 and LiH except for the VWN-MSM calculations where we encountered excessive problems with symmetry breaking and decided to use the same reference but with the **FOCK** option so that the VWN energies are evaluated using HF MOs. This is not expected to make much difference in a small highly symmetric molecule such as O_2 . The results are shown in **Fig. 32**. These calculations confirm that $B = A$ for the MSM-HF and both are roughly independent of R . For the MSM-VWN, B is approximately equal to, but smaller than, A for most R . So MSM-VWN is behaving roughly like MSM-HF and $B \approx A$ is a reasonable first approximation. For the EXACT calculations, both A and B decrease as R increases. This is not captured in our simple calculations, but we note that the MSM-DFT is able to give fairly good results compared to the EXACT results near the ground-state equilibrium bond length *provided* we are willing to climb Jacob's ladder and use more sophisticated functionals [16].

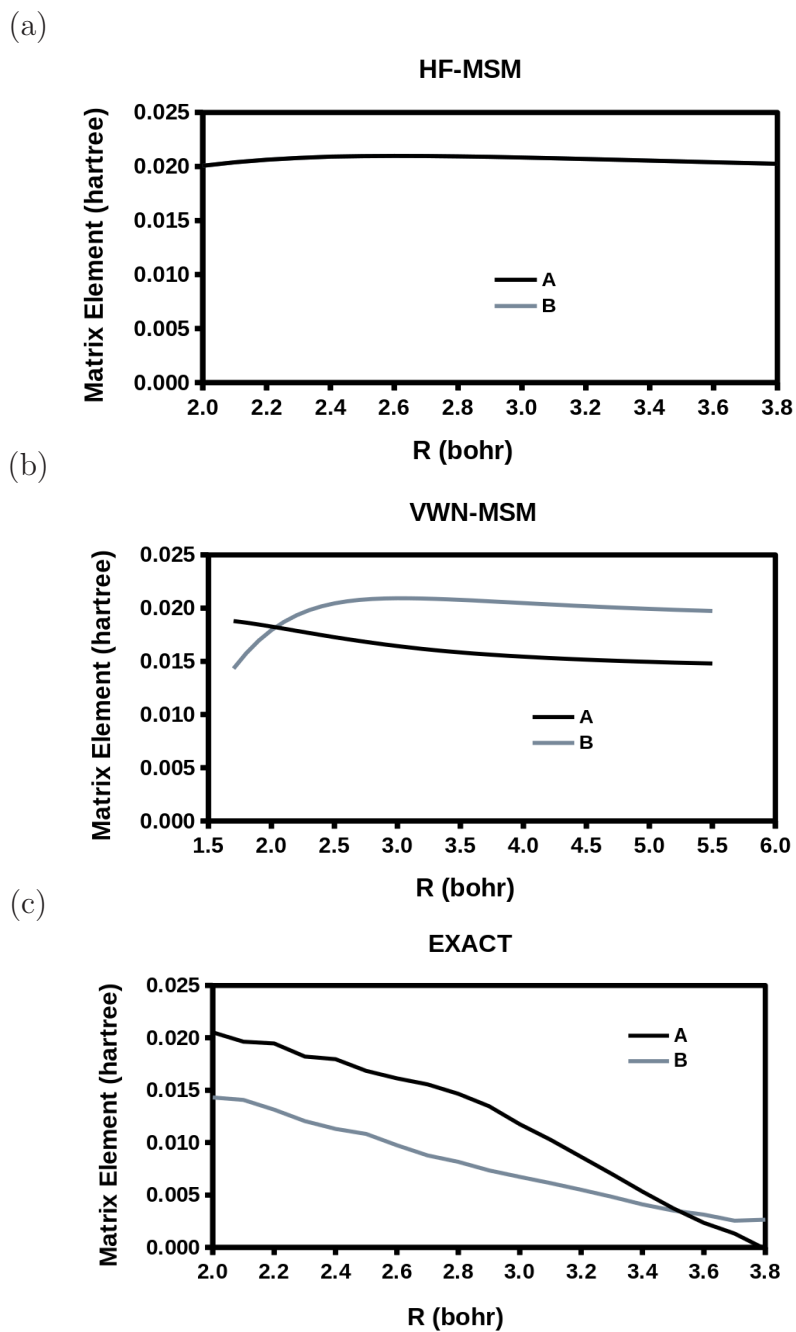


Figure 32: Plot of A and B as a function of bond distance R : (a) MSM-HF, (b) MSM-VWN, (c) EXACT. Note that the A and B lines are identical in part (a). The EXACT calculations are the same as the one used in Ref. [16]. The equilibrium bond length in the ground state is 2.3 bohr and it is very close to this value for the two excited states.

5 Concluding Discussion

This article began with a discussion of the need for a simple parameter-free way to incorporate static correlation into DFT as a way to overcome effective failures of NVR in practical applications of DFT, notably to photochemistry. DFT-MSM is a well-established symmetry-based method for introducing some multideterminantal character into DFT. It has some advantages in the simplicity with which it is able to treat charge transfer and (some) double excitations. It may be viewed as constructing and diagonalizing a small CI matrix from different occupations of frozen orbitals constructed from some “state-averaged” reference configuration. The diagonal elements are calculated using DFT with standard approximate xc-functionals. The off-diagonal elements could be calculated from WFT but we have shown in our examples that such matrix elements are rather inappropriate for use in MSM-DFT.

This article has presented a diagrammatic method for analyzing MSM-DFT with the lofty aim of freeing MSM-DFT from the symmetry-dependence of its traditional form. We emphasize that we are neither doing diagrammatic MBPT on top of DFT as would be done in *GW* or Bethe-Salpeter Green’s function calculations (e.g., Ref. [12]) nor are we adding MBPT corrections as in dressed TD-DFT (e.g., Ref. [14] and references therein). Instead, this is a tool for revealing “hidden” similarities between MSM-DFT and WFT. “Hidden” here means that rather than calculating the same object in two different ways, the object is playing the same role in the two theories. In particular, we see that certain terms in MSM-DFT can play a similar role in MSM-DFT as they do in WFT, even though we have no other justification for this than that the diagrams are similar.

We have given a few examples of MSM calculations for calculating the PECs of simple molecules within the TOTEM. A deliberate attempt was made to use only the simplest functionals, namely VWN and HF, as we wanted to keep our examples as elementary as possible. In general, the HF-MSM calculations do better at describing the shape of the open-shell singlet PECs in both H_2 and LiH. Surprisingly, the diagrammatic approach yields a simple but effective parameter-free way to dissociate H_2 without symmetry breaking. The same approach is not possible for LiH within the TOTEM as it would most likely require an expanded active space. On the other hand, the VWN-MSM describes charge transfer well which would not be the case in TD-DFT [44].

Diagrammatic MSM-DFT also suggests a way to carry out symmetry-free calculations for O_2 by equating $B = A$ (Subsec. 4.3). This necessarily means that degenerate states in O_2 will no longer be exactly degenerate, but this may be a small price to pay for enlarging the field of application of MSM-DFT beyond high-symmetry problems.

On the occasion of this *Festschrift* in honor of John P. Perdew’s 80th birthday, we think it appropriate to emphasize the parameter-free first principles approach taken here, even if not justified within formal DFT. John is one of the strongest advocates of creating *ab initio* functionals that fulfill as many conditions as possible that should be satisfied by the exact xc functional on the grounds that such a functional would be most likely to describe a variety of systems from atoms to molecules equally well. As discussed in the introductory section of this article, NVR is known to fail for many systems and effective failure of NVR is omnipresent in many photochemical applications of DFT because of the presence of strong static correlation effects due to quasi-degeneracies. Hence there is a need for a parameter-free multideterminantal DFT which includes static correlation. The present article does not yet meet that lofty ideal as we should show, for example, how to

go beyond the TOTEM and how gradients would be calculated before claiming to have a reasonably complete theory. However the present method, as far as we have gone, is indeed parameter-free and is, we think, not without merit as a step in the right direction.

Acknowledgements

The formal part of this project was initiated before the 7th African School on Electronic Structure Methods and Applications (ASESMA) which took place in Kigali, Rwanda, in 2023. However the numerical calculations began as an ASESMA project with the intent of doing research-level work that could be continued after ASESMA and submitted. Calculations were done on our personal computers running DEMON2K under LINUX. MEC is grateful to Anne Milet for financing his plane tickets to and from ASESMA. MEC and AP are grateful to Anne Justine Etindele for many helpful discussions. We are all grateful to Stephen Nyaranga for helpful discussions. He began this project with us but was unfortunately unable to continue. We are all grateful to the many people who have made this and previous ASESMA schools possible. They are too many to be named here.

Supplementary Information

- Multideterminantal Extensions to DFT
- Attempts to Unify TD-DFT and MSM-DFT
- LiH Example Calculations
- Proof of the Identical Nature of Two Expressions in the MSM-HF Treatment of O₂
- CRediT contributor roles [45].

References

- [1] W. Kohn and L. J. Sham, [Self-consistent equations including exchange and correlation effects](#), Phys. Rev. **140**, A1133 (1965).
- [2] P. Hohenberg and W. Kohn, [Inhomogenous electron gas](#), Phys. Rev. **136**, B864 (1964).
- [3] J. E. Harriman, [Orthonormal orbitals for the representation of an arbitrary density](#), Phys. Rev. A **24**, 680 (1981).
- [4] H. Englisch and R. Englisch, [Hohenberg-Kohn theorem and non- \$v\$ -representable densities](#), Physica **121A**, 253 (1983).
- [5] M. Levy, [Universal variational functionals of electron densities, first-order density matrices, and natural spin-orbitals and solution of the \$v\$ -representability problem](#), Proc. Nat. Acad. Sci. USA **76**, 6062 (1979).

- [6] M. Levy, [Electron densities in search of Hamiltonians](#), Phys. Rev. A **26**, 1200 (1982).
- [7] M. E. Casida and M. Huix-Rotllant, [Progress in time-dependent density-functional theory](#), Annu. Rev. Phys. Chem. **63**, 287 (2012).
- [8] E. Tapavicza, I. Tavernelli, U. Rothlisberger, C. Filippi, and M. E. Casida, [Mixed time-dependent density-functional theory/classical surface hopping study of oxirane photochemistry](#), J. Chem. Phys. **129**, 124108 (2008).
- [9] A. M. Teale et al., [DFT exchange: sharing perspectives on the workhorse of quantum chemistry and materials science](#), Phys. Chem. Chem. Phys. **24**, 28700 (2022).
- [10] T. Ziegler, A. Rauk, and E. J. Baerends, [On the calculation of multiplet energies by the Hartree-Fock-Slater method](#), Theor. Chim. Acta **4**, 877 (1977).
- [11] C. Daul, [Density functional theory applied to the excited states of coordination compounds](#), Int. J. Quantum Chem. **52**, 867 (1994).
- [12] G. Onida, L. Reining, and A. Rubio, [Electronic excitations: density-functional theory versus many-body Green's-function approaches](#), Rev. Mod. Phys. **74**, 601 (2002).
- [13] M. E. Casida and M. Huix-Rotllant, [Many-body perturbation theory \(MBPT\) and time-dependent density-functional theory \(TD-DFT\): MBPT insights about what is missing in, and corrections to, the TD-DFT adiabatic approximation](#), in *Density-Functional Methods for Excited States*, edited by N. Ferré, M. Filatov, and M. Huix-Rotllant, volume 361 of *Topics in Current Chemistry*, page 1, Springer, 2015.
- [14] M. Huix-Rotllant, A. Ipatov, A. Rubio, and M. E. Casida, [Assessment of dressed time-dependent density-functional theory for the low-lying valence states of 28 organic chromophores](#), Chem. Phys. **391**, 120 (2011).
- [15] I. Shavitt and R. J. Bartlett, *Many-Body Methods in Chemistry and Physics: MBPT and Coupled-Cluster Theory*, Cambridge University Press, Cambridge, England, UK, 2009.
- [16] A. Ponra, A. J. Etindele, O. Motapon, and M. E. Casida, [Practical treatment of singlet oxygen with density-functional theory and the multiplet-sum method](#), Theo. Chem. Acc. **140**, 154 (2021).
- [17] I. M. Gelfand and S. V. Fomin, *Calculus of Variations*, Prentice-Hall Inc., Englewood Cliffs, New Jersey, 1963, translated by R. A. Silverman.
- [18] A. M. Koster et al., [DEMON2K: density of Montreal, version 5.0](#), The deMon developers, Cinvestav, Mexico City (2018), http://www.demon-software.com/public_html/index.html, Last accessed 3 July 2021.
- [19] [Asema: African school on electronic structure methods and applications](#), <https://sites.google.com/site/asesmasite/>, Last accessed 27 June 2023.
- [20] M. E. Casida, [DEMON2K: Density-functional theory \(DFT\) for chemical physicists/physical chemists](#), http://www.demon-software.com/public_html/tutorials/main.pdf, accessed: 11 November 2022.

- [21] N. B. Oozeer, A. Ponra, A. J. Etindele, and M. E. Casida, [A new freely-downloadable hands-on density-functional theory workbook using a freely-downloadable version of DEMON2K](#), *Pure Appl. Chem.* **95**, 213 (2023).
- [22] S. H. Vosko, L. Wilk, and M. Nusair, [Accurate spin-dependent electron liquid correlation energies for local spin density calculations: a critical analysis](#), *Can. J. Phys.* **58**, 1200 (1980).
- [23] D. M. Ceperley and B. J. Alder, [Ground state of the electron gas by a stochastic method](#), *Phys. Rev. Lett.* **45**, 1697 (1980).
- [24] K. R. Lykke, K. K. Murray, and W. C. Lineberger, [Threshold photodetachment of \$H^-\$](#) , *Phys. Rev. A* **43**, 6104 (1991).
- [25] T. E. Sharp, [Potential-energy curves for molecular hydrogen and its ions](#), *Atomic Data* **2**, 119 (1971).
- [26] W. Kołos and L. Wolniewicz, [Potential energy curves for the \$X^1\Sigma_g^+\$, \$b^3\Sigma_u^+\$, and \$c^1\pi_u\$ states of the hydrogen molecule](#), *J. Chem. Phys.* **43**, 2429 (1965).
- [27] W. Kołos and L. Wolniewicz, [Potential-energy curve for the \$B^1\Sigma_u^+\$ state of the hydrogen molecule](#), *J. Chem. Phys.* **45**, 509 (1966).
- [28] W. Kołos and L. Wolniewicz, [Vibrational and rotational energies for the \$B^1\Sigma_u^+\$, \$c^1\pi_u\$, and \$a^3\sigma_g^+\$ states of the hydrogen molecule](#), *J. Chem. Phys.* **48**, 3672 (1968).
- [29] W. Kołos and L. Wolniewicz, [Theoretical investigation of the lowest double-minimum state \$e, f, ^1\sigma_g^+\$ of the hydrogen molecule](#), *J. Chem. Phys.* **50**, 3228 (1969).
- [30] W. Kołos and J. Rychlewski, [Ab initio potential energy curves and vibrational levels for the \$C\$ and \$D^1\Pi_u\$ states of the hydrogen molecule](#), *J. Mol. Spectrosc.* **62**, 109 (1976).
- [31] W. Kołos, [Ab initio potential energy curves and vibrational levels for the \$B''\$, \$b\$, and \$b'\$ states of the hydrogen molecule](#), *J. Mol. Spectrosc.* **62**, 429 (1976).
- [32] W. Kołos and J. Rychlewski, [Ab initio potential energy curves and vibrational levels for the \$c\$, \$l\$, and \$i\$ states of the hydrogen molecule](#), *J. Mol. Spectrosc.* **66**, 428 (1977).
- [33] L. Wolniewicz and K. J. Dressler, [The \$B^1\Sigma_u^+\$, \$B'^1\Sigma_u^+\$, \$C^1\Pi_u\$, and \$D^1\Pi_u\$ states of the \$H_2\$ molecule. Matrix elements of angular and radial nonadiabatic coupling and improved ab initio potential energy curves](#), *Chem. Phys.* **88**, 3861 (1988).
- [34] G. Staszewska and L. Wolniewicz, [Adiabatic energies of excited \$^1\Sigma_u\$ states of the hydrogen molecule](#), *J. Mol. Spectrosc.* **212**, 208 (2002).
- [35] L. Wolniewicz and G. Staszewska, [Excited \$^1\Pi_u\$ and the \$^1\Pi_u \rightarrow X^1\Sigma_g^+\$ transition moments of the hydrogen molecule](#), *J. Mol. Spectrosc.* **220**, 45 (2003).
- [36] C. Lee, Y. Gim, and T. H. Choi, [Calculation of potential energy curves of excited states of molecular hydrogen by multi-reference configuration-interaction method](#), *Bull. Korean Chem. Soc.* **34**, 1771 (2013).

- [37] M. E. Casida, F. Gutierrez, J. Guan, F. Gadea, D. R. Salahub, and J. Daudey, [Charge-transfer correction for improved time-dependent local density approximation excited-state potential energy curves: Analysis within the two-level model with illustration for H₂ and LiH](#), *J. Chem. Phys.* **113**, 7062 (2000).
- [38] C. A. Coulson, *Valence*, Clarendon Press, Oxford, England, UK, 1952.
- [39] H. W. Wasserman and J. L. Ives, [Singlet oxygen in organic synthesis](#), *Tetrahedron* **37**, 1825 (1981).
- [40] P. R. Ogilby, [Singlet oxygen: there is indeed something new under the sun](#), *Chem. Soc. Rev.* **39**, 3181 (2010).
- [41] A. A. Ghogare and A. Greer, [Using singlet oxygen to synthesize natural products and drugs](#), *Chem. Rev.* **116**, 9994 (2016).
- [42] M. Oelgemöller, [Solar photochemical synthesis: From the beginnings of photochemistry to the solar manufacturing of commodity chemicals](#), *Chem. Rev.* **116**, 9664 (2016).
- [43] J. Al-Nu'airat, I. Oluwoye, N. Zeinali, M. Altarawneh, and B. Z. Dlugogorski, [Review of chemical reactivity of singlet oxygen with organic fuels and contaminants](#), *The Chemical Record* **21**, 315 (2021).
- [44] J. I. Fuks, A. Rubio, and N. T. Maitra, [Charge-transfer in time-dependent density-functional theory via spin-symmetry breaking](#), *Phys. Rev. A* **83**, 042501 (2011).
- [45] [Credit \(contributor roles taxonomy\)](#), <https://credit.niso.org/>, Last accessed 11 August 2023.